MARTIN MARIETTA ENERGY SYSTEMS LIBRARIES

3 4456 0266737 1

ORNL/TM-10365

ornl

OAK RIDGE
NATIONAL
LABORATORY

MARTIN MARIETTA

Relative Merits of Size, Field, and Current on Ignited Tokamak Performance: A Comparison of "CITs" and "Super-JETs"

N. A. Uckan

OAK RIDGE NATIONAL LABORATORY
CENTRAL RESEARCH LIBRARY
CIRCULATION SECTION
4500N ROOM 175
LIBRARY LOAN COPY
DO NOT TRANSFER TO ANOTHER PERSON
If you wish someone else to see this report, send in name with report and the library will arrange a loan.

OPERATED BY
MARTIN MARIETTA ENERGY SYSTEMS, INC.
FOR THE UNITED STATES
DEPARTMENT OF ENERGY

Printed in the United States of America. Available from
National Technical Information Service
U.S. Department of Commerce
5285 Port Royal Road, Springfield, Virginia 22161
NTIS price codes—Printed Copy: A03; Microfiche A01

This report was prepared as an account of work sponsored by an agency of the United States Government. Neither the United States Government nor any agency thereof, nor any of their employees, makes any warranty, express or implied, or assumes any legal liability or responsibility for the accuracy, completeness, or usefulness of any information, apparatus, product, or process disclosed, or represents that its use would not infringe privately owned rights. Reference herein to any specific commercial product, process, or service by trade name, trademark, manufacturer, or otherwise, does not necessarily constitute or imply its endorsement, recommendation, or favoring by the United States Government or any agency thereof. The views and opinions of authors expressed herein do not necessarily state or reflect those of the United States Government or any agency thereof.

ORNL/TM-10365
Dist. Category UC-20 a,d,f,g

Fusion Energy Division

RELATIVE MERITS OF SIZE, FIELD, AND CURRENT ON IGNITED TOKAMAK PERFORMANCE: A COMPARISON OF "CITS" AND "SUPER-JETS"

N. A. Uckan

Date Published: August 1987

Prepared by the
OAK RIDGE NATIONAL LABORATORY
Oak Ridge, Tennessee 37830
operated by
MARTIN MARIETTA ENERGY SYSTEMS, INC.
for the
U.S. DEPARTMENT OF ENERGY
under contract DE-AC05-84OR21400

MARTIN MARIETTA ENERGY SYSTEMS LIBRARIES

3 4456 0266737 1

CONTENTS

ABSTRACT v
1. INTRODUCTION 1
2. POWER BALANCE EQUATION AND REGIMES OF PLASMA OPERATION 3
3. CONFINEMENT MODELS 6
4. IGNITION CONDITIONS AND PLASMA PERFORMANCE WITH OHMIC SCALINGS 8
4.1 Neo-Alcator-like global confinement scaling 8
4.2 Combined neoclassical ion and neo-Alcator electron scalings 13
5. PERFORMANCE WITH AUXILIARY SCALINGS 18
5.1 Kaye-Goldston L-mode (H-mode) scaling 18
5.2 Goldston L-mode (H-mode) scaling 21
5.3 Mirnov-like scaling 22
5.4 T-10/T-11 scaling 23
6. DISCUSSION 25
ACKNOWLEDGMENT 27
REFERENCES 29

ABSTRACT

A simple global analysis is used to examine the relative merits of size ($L = a$ or R_o), field (B_o), and current (I) on ignition regimes of tokamaks under various confinement scaling laws. Scalings of key parameters ($n\tau_E$, β, P_{aux}, P_{fus}, etc.) with L, B_o, and I are presented at several operating points, including (1) optimal path to ignition (saddle point), (2) ignition at minimum beta, (3) ignition at 10 keV, and (4) maximum performance at the limits of density ($n_{max} \sim B_o/R_o$) and beta ($\beta_{crit} \sim I/aB_o$). Expressions for the saddle point and the minimum conditions needed for Ohmic ignition are derived analytically for any confinement model of the form $\tau_E \sim n^x T^y$. For a wide range of confinement models, the "figure of merit" parameters $aB_o^2/q_* \sim IB_o(R_o/a)$ and I are found to give a good indication of the relative performance of the devices, where q_* is the cylindrical safety factor. As an illustration, the results are applied to "CITs" (a class of compact, high-field ignition tokamaks) and "Super-JETs" [a class of large-size (few $\times$ JET), low-field, high-current (20-MA) devices].

1. INTRODUCTION

The prospect of achieving ignition in a compact, high-density, high-field tokamak has long been advocated by Coppi [1] and Cohn et al. [2,3]. The IGNITOR [4] (one of the latest versions of the original IGNITOR discussed in Ref. [1]) and the U.S. Compact Ignition Tokamak (CIT) (a version of which is discussed in Ref. [5]) are two examples of this class of small ($R_o \sim 1$–2 m), high-power-density devices. In these devices sufficient confinement for ignition is attained through higher densities ($\langle n \rangle \sim 4$–10×10^{20} m^{-3}), magnetic fields ($B_o \sim 10$–13 T), and plasma currents ($I \sim 10$ MA) rather than through size scaling. The successful results obtained from high-field tokamak experiments are discussed in a recent review article by De Marco et al. [6]. Alternatively, the ignition conditions could also be achieved in a class of large-size, low-field, high-current devices, such as those considered for INTOR-class engineering test reactors (ETRs) [7]. The "Super-JET" [8], with $I \sim 20$ MA and a size of about 2.5 times that of JET, represents a unique, extreme example of this class of large, low-power-density devices. The Super-JET (considered as a possible reactor candidate in Ref. [8]) and IGNITOR (considered as a possible candidate for an ignition experiment by Coppi [1,4]) are both envisioned to reach ignition by Ohmic heating alone. To achieve Ohmic ignition, the use of super-high fields ($B_o \sim 15$–25 T) in compact devices has recently been considered in SHOT (**S**uper **H**igh-Field **O**hmically Heated **T**okamak) [9] and IGNITEX (**IGNIT**ion **EX**periment) [10] studies.

In this paper, a simple power balance equation (given in Section 2) is used to examine the relative merits of size ($L = a$ or R_o), field (B_o), and current (I) on ignited tokamak performance. The minimum conditions needed for ignition and, once ignited, the plasma performance within an ignited regime depend in part on the diffusive energy losses (χ_e and χ_i or τ_E). Although there is no universal model for these losses, various confinement scalings (given in Section 3) are used (in Sections 4 and 5) to illustrate the potential range of performance expected in devices with different parameters (L, B, I, etc.). The confinement scalings considered range from optimistic models based on ohmically heated plasmas to pessimistic models (L-mode scalings) that include confinement degradation by both auxiliary and fusion alpha heating. Favorable H-mode confinement is also considered. Of course, performance projections also depend on other factors, such as the inventiveness in plasma operation scenarios during startup, heating to ignition, etc., through tight control of profiles (e.g., n, J), sawtooth oscillations, etc. Here, in principle, such scenarios are assumed to apply across the board (i.e., independent of a given class of device) and are not considered.

As an illustration, the results of this study are applied to "CITs" [4,5] and "Super-JETs" [8]. Their parameters are summarized in Table I.

In all expressions, unless otherwise stated, the volume-averaged values for density ($\langle n \rangle$), density-averaged temperature ($\langle T \rangle = \langle nT \rangle / \langle n \rangle$), etc., are used (without the angle brackets). The units are MKS, with T in kilo electron volts, current I in megamperes, and power in megawatts. When designated, $n_{20} = n/10^{20}$ m^{-3} and $T_{10} = T/10$ keV.

TABLE I. MACHINE AND PLASMA PARAMETERS

	CIT-2[a]		IGNITOR	Super-JET	JET[b]
	Limiter	Divertor	(13.4 T)	(2.5 × JET)	(7 MA)
Major radius, R_o (m)	1.32	1.34	1.12	7.4	2.96
Minor radius, a (m)	0.43	0.41	0.42	3.0	1.2
Aspect ratio, A	3.1	3.25	2.65	2.46	2.46
Elongation/triangularity, κ/δ	2/0.4	2.1/0.4	1.7/0.22	1.7/? (0)	1.7/? (0)
Toroidal field, B_o (T)	10.4	10.3	13.4	4.0	3.45
Plasma current, I (MA)	10	9	11.25	20	7
Safety factor, $q_\psi(a)$	2.8	2.8[c]	2.6	3.2	3.2
Cylindrical q, q_*	2.2	2.3	1.95	2.35	2.3
Average poloidal field, $\bar{B}_\theta(a)$ (T)	2.7	2.45	3.72	0.96	0.84
Average current density, $\langle J \rangle$ (MA/m^2)	8.7	8.2	11.9	0.42	0.9
Density limit (10^{20} m^{-3})					
Murakami, $\langle n_{\rm mu} \rangle$	5.4	5.0	9.2	0.35	0.75
Greenwald, $\langle n_{\rm GR} \rangle$	10.5	10.1	12.2	0.42	0.93
Troyon beta limit, $\beta_{\rm crit}$ (%)	6.75	6.4	6.0	5.0	5.1
Figures of merit					
$aB_o^2/q_* \equiv X_{\rm m}$	21.1	18.7	38.5	20.3	6.1
$I\bar{B}_\theta$ (IB_o)	27 (104)	22 (93)	42 (150)	19 (80)	6 (24)
aB_o (q_*AI)	4.4 (68)	4.2 (68)	5.6 (58)	12 (116)	4.1 (40)
B_o/R_o	7.85	7.7	12	0.54	1.2
Plasma surface area, S (m^2)	39	39	27	1225	196
Plasma volume, V (m^3)	9.5	9.2	6.6	2235	143

[a] A version of the U.S. Compact Ignition Tokamak design [5]. At present, several variations (large a and R_o, smaller κ, larger q_ψ, etc.) are being considered

[b] JET parameters are included here only to demonstrate its relation to Super-JET.

[c] Defined at 96% flux surface.

2. POWER BALANCE EQUATION AND REGIMES OF PLASMA OPERATION

To establish the conditions under which ignition can be achieved, either with the aid of auxiliary heating (a general case) or with Ohmic heating alone (a special case), we use a simple global power balance equation,

$$F = \frac{\partial W}{\partial t} = -P_{\rm con} - P_{\rm rad} + P_\alpha + P_{\rm OH} + P_{\rm aux} \tag{1}$$

where W is the total plasma energy and the terms on the right-hand side represent the power loss due to transport processes ($P_{\rm con} = P_e + P_i$), the bremsstrahlung radiation ($P_{\rm rad}$), the alpha power (P_α), the Ohmic power ($P_{\rm OH}$), and the auxiliary power ($P_{\rm aux}$). Here, synchrotron radiation and impurity line radiation are neglected. In a dense, relatively clean plasma, the line radiation plays a small role in the central (burn) region of the plasma. Although the synchrotron radiation could represent a large power loss (at high burn temperatures, $T > 15$ keV) in fusion plasmas with high magnetic fields and low wall reflectivity ($\Re$), it is typically smaller than the bremsstrahlung radiation for ignition temperatures $T \sim 5$–10 keV, provided that $B_{\rm o} < 15$ T and $\Re > 0.9$. At higher burn temperatures, this loss process could provide some passive thermal stabilization.

A typical set of steady-state ($F = 0$) plasma parameter curves (known as Cordey plots [11] or plasma operation contours, POPCONs [12]) in density-temperature (n-T) space is shown in Fig. 1. In steady state, the ignition condition (curve 1) is $F = P_{\rm aux} = 0$; $P_{\rm con} + P_{\rm rad} = P_\alpha + P_{\rm OH}$. At low enough temperatures, this equation can also be satisfied, corresponding to Ohmic (OH) equilibrium (curve 2). The thermal runaway (curve 3) is defined as $F = \partial F/\partial T = \partial P_{\rm aux}/\partial T = 0$, which is satisfied at $T(n) = T_*(n)$, where $P_{\rm aux} = P_{\rm aux}(\max)$ along a line of constant density. The optimal path to ignition (saddle point—point A) is determined from $F = \partial F/\partial T = \partial F/\partial n = 0$, which is satisfied at (n_*, T_*) where $P_{\rm aux}(\max)$ is minimum. At (n_*, T_*), if $P_{\rm aux} = 0$, this gives the optimal (minimum) condition for Ohmic ignition ($F = P_{\rm aux} = \partial F/\partial T = \partial F/\partial n = 0$). Also shown in Fig. 1 are the density limit ($n_{\rm max} \sim B_{\rm o}/R_{\rm o}$) [13] and the beta limit ($\beta_{\rm crit} \sim I/aB_{\rm o}$) [14], both of which constrain the ignited operating window (dotted region). The size of this operating window $(\Delta n,\ \Delta T)_{\rm op}$ is a measure of the ignition margin, which is defined here as $M_I = (P_\alpha + P_{\rm OH})/(P_{\rm con} + P_{\rm rad})$.

For any confinement model of the form $\tau_E \sim n^x T^y f(\text{others})$, the optimal path (saddle point) is determined from [15]

$$\begin{aligned} [(1+x)/2]P_{\rm con} &= P_{\rm aux} + P_{\rm OH} \\ [(1-x)/2]P_{\rm con} &= P_\alpha - P_{\rm rad} \\ 2(1-y)P_{\rm con} &= 2sP_\alpha - 3P_{\rm OH} - P_{\rm rad} \end{aligned} \tag{2}$$

where $s = \partial \ln\langle\sigma v\rangle_{\rm DT}/\partial \ln T \sim 3$ for $T < 10$ keV. As mentioned, if $P_{\rm aux} = 0$, then Eq. (2) gives the minimum condition for Ohmic ignition.

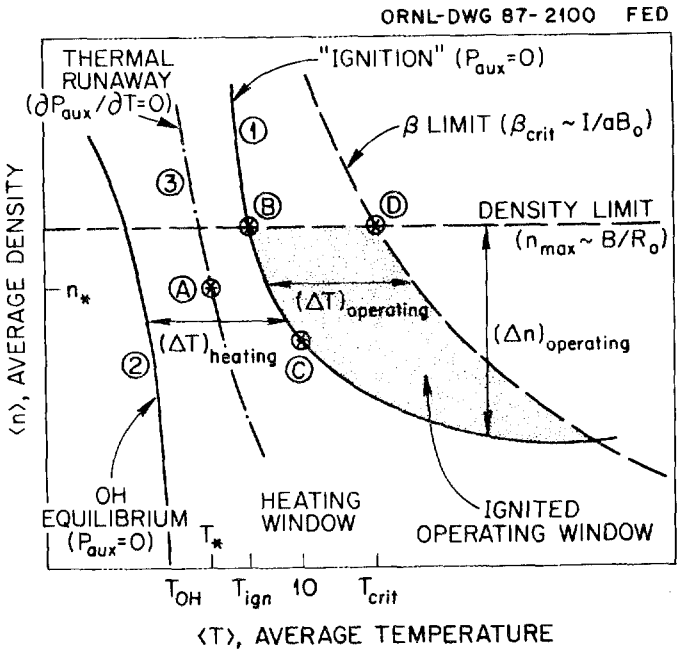

Fig. 1. A typical plasma parameter operating space, showing ignition (curve 1), OH equilibrium (curve 2), and thermal runaway (curve 3) contours. Also shown are the limits imposed on density ($n < n_{\max} \sim B_o/R_o$) and total plasma beta ($\beta < \beta_{\text{crit}} \sim I/aB_o$). Operating points:
(A) optimal path to ignition (n_*, T_*);
(B) ignition at $n \sim n_{\max}$, $T = T_{\text{ign}}$ (min);
(C) ignition at $T = 10$ keV;
(D) maximum performance at $n = n_{\max}$, $\beta = \beta_{\text{crit}}$ ($T = T_{\text{crit}}$).
The heating window and the ignited operating window (dotted region) are indicated.

To compare the relative merits and potential of devices with different parameters and to identify classes of devices with similar (or different) characteristics, it is useful to consider the scaling of various key parameters ($n\tau_E$, P_{aux}, β, P_{fus}, $L_w \sim P_{\text{fus}}/\text{area}$, etc.) with B, L, and/or I at various operating points. Several operating points are shown in Fig. 1: (A) along the optimal path to ignition (saddle point — n_*, T_*); (B) ignition at $n \sim n_{\max}$, $T = T_{\text{ign}}$(min); (C) ignition at $T = 10$ keV; and (D) maximum parameters at $n = n_{\max}$, $\beta = \beta_{\text{crit}}$ ($T = T_{\text{crit}}$). Here the maximum density is given by the Murakami limit [13], taken as

$$n_{e\max} = \langle n_{\text{mu}} \rangle = 1.5 \times 10^{20}\ B_o/R_o q_* \ (\text{m}^{-3}) \tag{3}$$

and the maximum volume-averaged beta is constrained by the Troyon-Gruber limit [14], taken as

$$\beta < \beta_{\text{crit}} = 3 \times 10^{-2} I/aB_o \tag{4}$$

where the current (I) is in megamperes (MA) and $\beta = \beta_e + \beta_i + \beta_{f\alpha} = \beta_{\rm th}(1+\gamma_{f\alpha})$, with $\beta_{\rm th} = \beta_e + \beta_i$ and $\gamma_{f\alpha} = \beta_{f\alpha}/\beta_{\rm th}$ the ratio of the fast alpha pressure to the plasma thermal pressure. The cylindrical equivalent safety factor q_* is [15]

$$q_* = (5a^2 B_o/IR_o)\ [(1+\kappa_*^2)/2] \tag{5}$$

where κ_* is an effective plasma elongation, corrected for plasma triangularity δ with $(\oint\ dl_\theta/2\pi a)^2 \simeq [1+\kappa^2(1+2\delta^2)]/2$ for small δ (< 0.35).

For simplicity, taking $T_e \simeq T_i \simeq T$, assuming profiles of the form $x = x_o(1 - r^2/a^2)^{\alpha_x}$, $x = n,\ T,\ J$, with $\alpha_J \sim 3\alpha_T/2$, and averaging Eq. (1) over the plasma cross section yields [15] (in MW/m^3)

$$\begin{aligned} F = &-0.24\ n_{20}^2 T_{10}(1+n_i/n_e)/(n_{20}\tau_E) - C_B n_{20}^2 T_{10}^{1/2} \\ &+ C_\alpha\ n_{20}^2 (T_{10}/T_{10C})^s + C_{\rm OH}\bar{\gamma}_{\rm NC} T_{10}^{-3/2}(B_o^2/q_o^2 R_o^2) + P_{\rm aux}/V \end{aligned} \tag{6}$$

where $\bar{\gamma}_{\rm NC} \simeq 2.5 \pm 0.3$ for $A = R_o/a \simeq 3 \mp 0.5$ (the average neoclassical resistivity enhancement factor), and $q_o = q(0)$ is the safety factor on axis. The coefficients $C = C(\alpha_n,\ \alpha_T,\ Z_{\rm eff},\ \kappa = b/a)$ and $\langle\sigma v\rangle_{\rm DT} \sim T_{10}^s$, where $s = 3$ for $T_{10} < T_{10C}$ and $s = 2$ for $T_{10C} < T_{10} < 2T_{10C}$, with T_C ($= 10T_{10C}$) $\sim f(\alpha_n,\ \alpha_T) \sim$ 7–10 keV. For $\alpha_n \sim 0.5$, $\alpha_T = 1.0$, and $Z_{\rm eff} \sim 1.5$ ($n_i/n_e \sim 0.9$), these coefficients are $C_B \sim 2.67 \times 10^{-2}$, $C_\alpha \simeq 0.1$, $T_{10C} \simeq 0.75$, and $C_{\rm OH} \simeq 8 \times 10^{-4}[(1+\kappa_*^2)/2\kappa]^2$. Equation (5) is further simplified by introducing a normalized density $m = n/n_{\rm max} = n_{20}/(1.5B_o/R_o q_*)$, where $m < 1$ identifies a density regime below the Murakami limit [Eq. (3)] and $m > 1$ a regime above the limit. The resulting equation is [15]

$$F = -f_{\rm con}(m,\ T_{10},\ n\tau_E) - a_B m^2 T_{10}^{1/2} + a_\alpha m^2 (T_{10}/0.75)^s + a_{\rm OH} T_{10}^{-3/2} + a_{\rm aux} = 0 \tag{7}$$

where

$$\begin{aligned} f_{\rm con}(m,\ T_{10},\ n\tau_E) &= 0.54 m^2 T_{10}(1+f_{nT})/(n_{20}\tau_E) \\ &= 1.8 m^2 T_{10}[(\chi_e/n_{20}a^2) + f_{nT}(\chi_i/n_{20}a^2)][(1+\kappa_*^2)/2\kappa^2] \end{aligned} \tag{8a}$$

$$a_B = (1.5)^2 C_B \simeq 6 \times 10^{-2}(Z_{\rm eff}/1.5) \tag{8b}$$

$$a_\alpha = (1.5)^2 C_B \simeq 0.225(f_{nT}/0.9)^2 \tag{8c}$$

$$\begin{aligned} a_{\rm OH} &= (q_*^2/q_o^2)\bar{\gamma}_{NC} C_{\rm OH} \\ &= 8 \times 10^{-4}(q_*^2/q_o^2)\bar{\gamma}_{NC}(Z_{\rm eff}/1.5)[(1+\kappa_*^2)/2\kappa]^2 \end{aligned} \tag{8d}$$

$$\begin{aligned} a_{\rm aux} &= P_{\rm aux}/[(B_o/R_o q_*)^2 V] \\ &= P_{\rm aux}/[(aB_o^2/q_*)(2\pi^2\kappa/q_* A)] \end{aligned} \tag{8e}$$

Here $f_{nT} = (n_i/n_e)(T_i/T_e) \simeq n_i/n_e \simeq 0.9$ for $Z_{\rm eff} = 1.5$ (with $Z \sim 6$) and $s = 3$ (2) for $T < 7.5$ keV ($T > 7.5$ keV). In Eq. (8a) the conduction losses are given in terms of the global energy confinement time (τ_E) and the electron (χ_e) and ion (χ_i) thermal diffusivities.

For a given geometry ($A = R_o/a$, κ) and plasma composition ($Z_{\rm eff}$), Eq. (7) depends only on m, T, and $n\tau_E$. For a wide range of confinement models of the form $\tau_{E\rm OH}$(neo-Alcator) $\sim nL^3$ and/or $\tau_{E\rm aux}$(L-/H-modes) $\sim LIf(P)$ with $f(P) \sim P^{-\alpha}$ or $\sim (C_1 + C_2/P)$; $n\tau_E \sim f(m)LB_o^2 \sim f(m)B_oI$ with $f_{\rm OH}(m) \sim m^2$ and $f_{\rm aux}(m) \sim m^z$, $z = (1-2\alpha)/(1-\alpha)$. Thus, for these forms of scalings, the power balance equation [Eq. (7)] is $F(m = \langle n\rangle/n_{\rm max},\ T,\ X_m) = 0$, where the "figure of merit" parameter $X_m = f(n\tau_E) \sim LB_o^2 \sim B_oI$. The plasma performance (ignition) contours in m-T space (see Fig. 1) will be the same for devices with similar X_m. That is, curves 1, 2, and 3; $T_{\rm OH}$, T_*, and $T_{\rm ign}$; and $P_{\rm fus}$ at points A, B, and C will be similar except for β and wall loading L_w.

From Eqs (3)–(5), in m-T space the $\beta_{\rm tot} = \beta_{\rm crit}$ contour is

$$mT_{10}(1+\gamma_{f\alpha}) \simeq 2.6\times 10^{-2}\ q_*IA \simeq 0.13aB_o[(1+\kappa_*^2)/2] \tag{9}$$

and

$$\beta_{\rm th} = \beta_e + \beta_i = 1.15\ mT_{10}/(q_*R_oB_o) \tag{10}$$

Typically, $\gamma_{f\alpha} \sim$ 5–25% for $T \sim$ 6–16 keV. At $n = n_{\rm max}(m=1)$, $\beta = \beta_{\rm crit}$ (point D in Fig. 1), and $T = T_{\rm crit} \propto IA$. Within the ignited operating window, $T \geq 10$ keV requires $q_*IA > 40$ (i.e., $I > 7$ MA for $A \sim 3$, $q_* \sim 2$).

3. CONFINEMENT MODELS

The following confinement models are used to illustrate the potential range of performance of ignited tokamaks.

Ohmic Heating — Neo-Alcator-Like Scaling [16] (τ_E or τ_{Ee}):

One of several variations of this scaling is given by

$$\begin{aligned} \tau_{\rm OH} &= \tau_{\rm NA} = 0.07 n_{20} a R_o^2 q_* \quad \text{(seconds)} \\ n_{20}\tau_{\rm NA} &\simeq 0.16\ {\rm m}^2(aB_o^2/q_*) \end{aligned} \tag{11}$$

Auxiliary Heating — L-Mode (H-Mode) Scalings [16] (τ_E or τ_{Ee}):

The general form of these scalings is

$$\tau_{\rm aux} \sim L^{(0.5-1.5)} I^{(0.6-1.5)} A_i^{(0.5-1.0)} \kappa^{(0.2-0.5)} \left[P^{-(0.3-0.6)} \text{ or } C_1 + C_2/P\right] \tag{12}$$

where A_i is the ion atomic mass number and P is the total heating power ($P_{\rm OH} + P_\alpha + P_{\rm aux} - P_{\rm rad}$). Typically $\tau_{\rm aux}$(H-mode) $\sim$ (2–3)$\tau_{\rm aux}$(L-mode). Specific examples follow.

1. Kaye-Goldston (KG) Scaling [17]

$$\tau_{\rm KG} = 0.056 f_{\rm LH} I^{1.24} P^{-0.58} R_{\rm o}^{1.65} a^{-0.49} \kappa^{0.28} n_{20}^{0.26} B_{\rm o}^{-0.09} (A_i/1.5)^{0.5}$$
$$\Rightarrow 5.3 \times 10^{-5}\ f_{\rm LH}^{2.4} I^{2.95} R_{\rm o}^{2.55} (A_i/1.5)^{1.2} / \left(n_{20}^{0.76} T_{10}^{1.38} a^{3.93} B^{0.21} \kappa^{0.71}\right) \tag{13a}$$

$$n_{20}\tau_{\rm KG} \simeq \frac{m^{0.25}}{80 T_{10}^{1.38}}\ f_{\rm LH}^{2.4} \left(\frac{aB_{\rm o}^2}{q_*}\right)^{1.5} \left(\frac{1+\kappa_*^2}{2}\right)^3 \frac{1}{\kappa^{0.7}} \left[\frac{(a/R_{\rm o})^{0.65}}{a^{0.2}\ q_*^{1.7}}\right]$$
$$\propto m^{0.25} I^3 (R_{\rm o}/a)^{2.3} a^{-1.65}\ , \tag{13b}$$

where $f_{\rm LH} = 1$ (L-mode) or ≥ 2 (H-mode) and $A_i = 2.5$.

2. Goldston (G) Scaling [18]

$$\tau_{\rm G} \simeq 0.037 f_{\rm LH} I P^{-0.5} R_{\rm o}^{1.75} a^{-037} \kappa^{0.5} (A_i/1.5)^{0.5}$$
$$\Rightarrow 1.52 \times 10^{-4}\ f_{\rm LH}^2 I^2 R_{\rm o}^{2.5} (A_i/1.5)/(n_{20} T_{10} a^{2.74}) \tag{14a}$$

$$n_{20}\tau_{\rm G} \simeq 2.53 \times 10^{-4} (m^0/T_{10}) f_{\rm LH}^2 I^2 (R_{\rm o}/a)^{2.5} a^{-0.24}$$
$$\simeq 6.34 \times 10^{-3} (m^0/T_{10}) f_{\rm LH}^2 (aB_{\rm o}^2/q_*) \left[(1+\kappa_*^2)/2\right]^2 \left[a^{0.75} (R_{\rm o}/a)^{0.5}/q_*\right] \tag{14b}$$

3. "Mirnov-Like" Scaling ($\tau_{\rm MI} \sim LI$)

For $L = a$, the scaling from various devices is [16]

$$\tau_{{\rm MI}a} \simeq (0.05\text{–}0.15) f_{\rm LH} a I$$
$$n_{20}\tau_{{\rm MI}a} \simeq (0.08\text{–}0.22) m f_{\rm LH}\ B_{\rm o} I/q_* (R_{\rm o}/a) \tag{15}$$
$$\simeq (0.4\text{–}1.1)\ m f_{\rm LH} (aB_{\rm o}^2/q_*)[(1+\kappa_*^2)/2]/q_* (R_{\rm o}/a)^2$$

For $L = R_{\rm o}$,

$$\tau_{{\rm MI}R_{\rm o}} \simeq (0.02\text{–}0.05)\ f_{\rm LH} R_{\rm o} I$$
$$n_{20}\tau_{{\rm MI}R_{\rm o}} \simeq (0.03\text{–}0.08) m f_{\rm LH}\ B_{\rm o} I/q_* \tag{16}$$
$$\simeq (0.15\text{–}0.4)\ m f_{\rm LH} (aB_{\rm o}^2/q_*)[(1+\kappa_*^2)/2]/q_* (R_{\rm o}/a)$$

The isotope (A_i) and plasma shape (κ) effects are included in the coefficients. The scalings of these forms represent the limit of the offset-linear forms of power degradation $\tau \sim (C_1 + C_2/P) LI \rightarrow C_1 LI$. In many H-mode discharges ($f_{\rm LH} \geq 2$), power degradation appears to be absent and $\tau_E \sim LI$, provided $\beta \ll \beta_{\rm crit}$ [16].

T-10/T-11 Scalings [19] (τ_{Ee}):

This scaling (known as the Mukhovatov-Merezhkin scaling) is similar to the Ohmic (OH), neo-Alcator scaling [Eq. (11), $\tau \sim nL^3$] with added $f(T_e)$ to account for confinement degradation:

$$\tau_{Ee} = \tau_{\rm MM} \simeq 3.5 \times 10^{-3}\ \bar{n}_{20} a^{0.25} R_{\rm o}^{2.75} q_* T_{10}^{-0.5} A_i^{0.5} \tag{17}$$

Taking $\tau_E \simeq f_\tau \tau_{Ee}$, $f_\tau \sim 1$–2 , and $\bar{n} = 1.2\langle n \rangle$ (for $\alpha_n \sim 0.5$),

$$n_{20}\tau_E = f_\tau n_{20} \tau_{\rm MM} \simeq 1.5 \times 10^{-2} f_\tau (m^2/T_{10}^{0.5})(aB_{\rm o}^2/q_*)(R_{\rm o}/a)^{0.75} \tag{18}$$

Ion Neoclassical (Chang-Hinton) Scaling [20] (τ_{Ei}):

The ion neoclassical thermal diffusivity is given by $\chi_i = f_{ix}\chi_{\rm CH}$. In the low-collisionality, banana regime,

$$\chi_{\rm CH}\ ({\rm m}^2/{\rm s}) \simeq 1.5 \times 10^{-2}\ K_2^* \frac{n_{20} Z_{\rm eff} q_*^2 A_i^{0.5}}{\epsilon^{3/2} T_{10}^{1/2} B_{\rm o}^2} \left(\frac{2}{1+\kappa_*^2}\right) \tag{19a}$$

where $K_2^* = (0.66 + 1.88\epsilon^{1/2} - 1.54\epsilon)(1 + 1.5\epsilon^2)$, $\epsilon = r/R_{\rm o}$, and f_{ix} is the neoclassical multiplier (anomaly). Thus,

$$\begin{aligned} n_{20}\tau_{Ei} &\simeq 20 T_{10}^{1/2} (aB_{\rm o}^2/q_*)[\epsilon^{3/2}\kappa^2 a/q_* Z_{\rm eff} A_i^{0.5} K_2^*]/f_{ix} \\ &\simeq 0.8 T_{10}^{1/2} I^2 (R_{\rm o}/a)^{0.5} [2\kappa/(1+\kappa_*^2)]^2 / Z_{\rm eff} A_i^{0.5} K_2^* f_{ix} \end{aligned} \tag{19b}$$

The OH scaling given by Eq. (11) does not yield the observed saturation of confinement at high density or degradation of confinement with auxiliary heating and is therefore considered an optimistic model. The scalings given by Eqs (12)–(14) include degradation of $\tau_{E\rm aux}$ with total power and thus represent a pessimistic model. In many recent experiments [16], although τ_E degrades with power, the observed confinement times are higher than that predicted from $\tau_{\rm KG}$, Eq. (13), or $\tau_{\rm G}$, Eq. (14). Because the OH scalings represent an upper limit to τ_E, a combination of OH and auxiliary scalings is taken [18],

$$\tau_E = \left(\tau_{E\rm OH}^{-2} + \tau_{E\rm aux}^{-2}\right)^{-1/2} \tag{20}$$

4. IGNITION CONDITIONS AND PLASMA PERFORMANCE WITH OHMIC SCALINGS

4.1. Neo-Alcator-like global confinement scaling

First, it is informative to look at a simple case where $\chi_e \sim \chi_i \sim \chi_{\rm NA}$, namely, $\tau_E \sim \tau_{E\rm OH} \sim \tau_{\rm NA}$ [Eq. (11)]. Substituting Eqs (8a) and (11) into Eq. (7) yields

$$F = -a_{\rm NA} T_{10} - a_B m^2 T_{10}^{1/2} + a_\alpha m^2 (T_{10}/0.75)^s + a_{\rm OH} T_{10}^{3/2} + a_{\rm aux} = 0 \tag{21}$$

where a_B, a_α, $a_{\rm OH}$, and $a_{\rm aux}$ are given in Eq. (8) and

$$a_{\rm NA} \equiv a_E/(aB_{\rm o}^2/q_*) \simeq 6.5/(aB_{\rm o}^2/q_*) \tag{22}$$

($s = 3$ for $T_{10} < 0.75$, $s = 2$ for $T_{10} > 0.75$.) Equation (21) can be solved analytically, with $m = f(T,\ aB_o^2/q_*)$, and the solution is nearly independent of any other parameter for a given geometry (κ, $A = R_o/a$). The minimum value of aB_o^2/q_* needed for ignition ($F = P_{aux} = 0$), subject to the density ($m < 1$) and beta ($\beta < \beta_{crit}$; $T < T_{crit}$) limits, is $aB_o^2/q_* \sim 12$ (16), requiring a plasma current (for $A \sim 3$) $I \sim 10$ (7) MA. For $aB_o^2/q_* > (aB_o^2/q_*)_{min}$, there is an ignited operating window, the size of which is determined by the plasma current [β_{crit}, see Eq. (19)].

Figure 2 shows (in m-T space) the steady-state ignition and OH equilibrium contours in the CIT, IGNITOR, and Super-JET machines (see Table I). Also shown are the $\beta = \beta_{crit}$ contours. The CIT and Super-JET have comparable $aB_o^2/q_* \sim 20$ and thus have similar ignition contours, as predicted by Eq. (21). The IGNITOR, with nearly twice the aB_o^2/q_* value (~39), ignites at a lower temperature and has a larger density operating window. Although all three devices have comparable $\beta_{crit} \sim 5$–6%, the Super-JET with 20 MA (nearly twice the current in CIT and IGNITOR) exhibits a larger temperature operating window ($T_{crit} \sim I$). Also, the minimum β at ignition is lower (far from β_{crit}) in Super-JET. Figure 3 shows (in n-T space) the ignition and auxiliary power contours. The parameters corresponding to various operating points are summarized in Table II. The scalings of various key parameters (listed in Table II) are as follows.

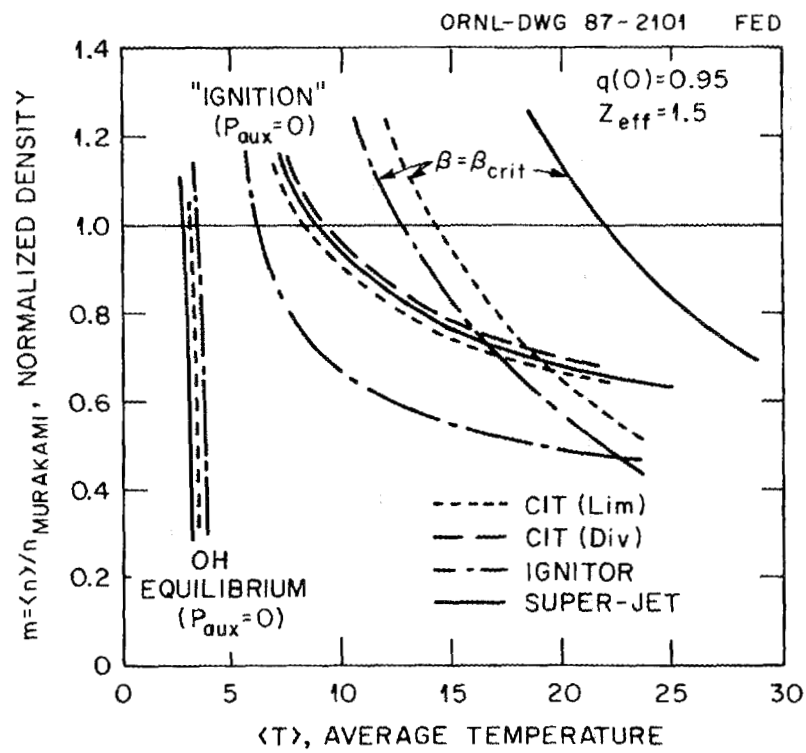

Fig. 2. Steady-state ignition and Ohmic equilibrium contours (in m-T space) for CIT, IGNITOR, and Super-JET with neo-Alcator (NA) global confinement scaling ($X_e \sim X_i \sim X_{NA}$; $\tau_E = \tau_{NA}$). The reference Murakami density limit is used ($m = n/n_{mu}$) and $\beta = \beta_{crit}$ contours are shown for all three cases. [$Z_{eff} \simeq 1.5$ and $q(0) \simeq 0.95$.]

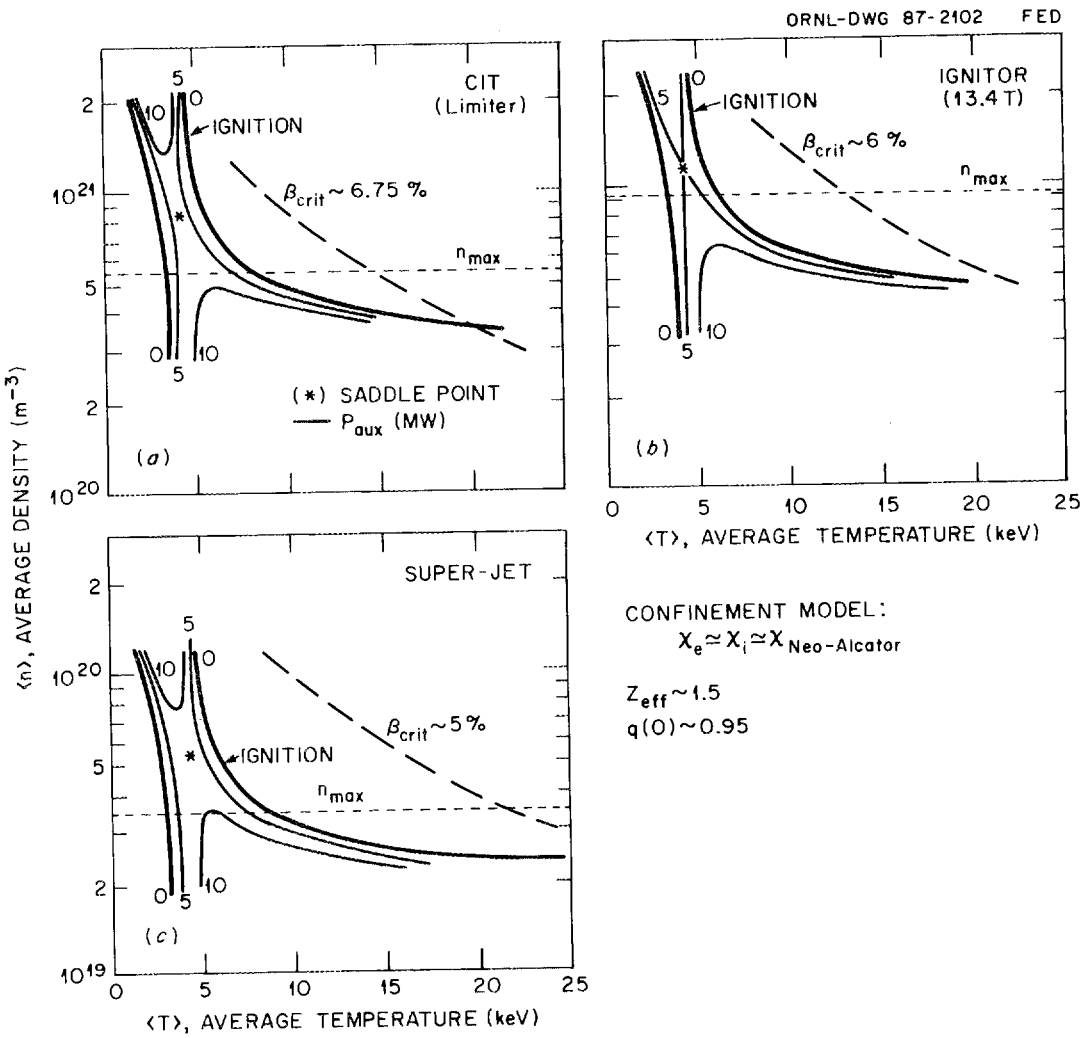

Fig. 3. Steady-state auxiliary power contours for (a) CIT, (b) IGNITOR, and (c) Super-JET with neo-Alcator (NA) global confinement scaling ($\chi_e \simeq \chi_i \simeq \chi_{NA}$; $\tau_E = \tau_{NA}$).

TABLE II. STEADY STATE, VOLUME-AVERAGED PARAMETERS AT VARIOUS OPERATING POINTS FOR NEO-ALCATOR-LIKE GLOBAL CONFINEMENT

SCALING: $\chi_e \sim \chi_i \sim \chi_{NA}(\tau_E \simeq \tau_{NA})$

	CIT-2		IGNITOR	Super-JET
	Limiter	Divertor	(13.4 T)	(2.5 × JET)
OH equilibriuim				
T_{OH} (keV)	3.5	3.5	3.7	3.2
Along optimal path (n_*, T_*)				
T_* (keV)	4.2	4.2	4.2	4.2
n_* (10^{20}m^{-3})	8.7	8.6	11.3	0.54
$m_* = n_*/\langle n_{mu}\rangle$	1.6	1.7	1.2	1.56
β_{th*} (%)	2.6	2.6	2.0	1.1
P_{fus*} (MW)	60	60	65	55
L_{w*} (MW/m^2)	1.55	1.55	2.45	0.045
Min P_{aux*} (MW)	6	5	5	8
At ignition ($m = n/n_{mu} = 1$)				
T (keV)	8.5	9.4	6.1	8.9
β_{th} (%)	3.25	3.4	2.4	1.45
β_{pol}	0.48	0.6	0.3	0.26
P_{fus*} (MW)	180	180	150	180
L_w (MW/m^2)	4.6	4.6	5.6	0.15
At ignition ($T = 10$ keV)				
n (10^{20} m^{-3})	4.95	4.85	6.2	0.32
β_{th} (%)	3.5	3.5	2.65	1.55
β_{pol}	0.52	0.62	0.34	0.27
P_{fus} (MW)	210	195	225	210
L_w (MW/m^2)	5.4	5.0	8.3	0.17
At $n = n_{mu}$, $\beta_{tot} = \beta_{crit}$				
T_{crit} (keV)	14.5	14.5	12.8	21.9
β_{th} (%)	5.5	5.2	5.0	3.6
β_{pol}	0.81	0.92	0.65	0.82
P_{fus} (MW)	480	400	800	770
L_w (MW/m^2)	12.3	10.2	30	0.63

The OH equilibrium temperature is

$$\begin{aligned} T_{10}(\mathrm{OH}) &\simeq (a_{\mathrm{OH}}/a_{\mathrm{NA}})^{0.4} \\ &\simeq 2.3\times 10^{-2}(aB_{\mathrm{o}}^2/q_*)^{0.4}(\bar{\gamma}_{\mathrm{NC}}Z_{\mathrm{eff}}q_*^2/q_{\mathrm{o}}^2)^{0.4}[(1+\kappa_*^2)/2\kappa]^{0.8} \end{aligned} \tag{23}$$

In Figs 2 and 3 (and Table II), $Z_{\mathrm{eff}} \simeq 1.5$, $q_{\mathrm{o}} \simeq 0.95$, and $\bar{\gamma}_{\mathrm{NC}} \sim f(A) \simeq 2.5$ for CIT, 2.7 for IGNITOR, and 2.8 for Super-JET.

The optimal path (m_*, T_*) is determined from Eq. (2), where $x = 1$, $y = 0$, $s = 3$, and $\bar{a}_\alpha = a_\alpha/(0.75)^3$:

$$T_{10*} = (a_B/\bar{a}_\alpha)^{0.4} \simeq 0.42(Z_{\mathrm{eff}}/1.5)^{0.4} \tag{24a}$$

$$m_*T_{10*} = [0.6(a_{\mathrm{OH}}/a_B) + 0.4(a_{\mathrm{NA}}/\bar{a}_\alpha)]^{0.5} \tag{24b}$$

$$\begin{aligned} P_{\mathrm{aux}*}(\mathrm{min}) &= (P_{\mathrm{con}} - P_{\mathrm{OH}}) \ \text{ at } \ (n_*,\ T_*) \\ &\simeq (2\pi^2\kappa/q_*A)(aB_{\mathrm{o}}^2/q_*)a_{\mathrm{NA}}T_{10*}[1 - T_{10*}^{-5/2}a_{\mathrm{OH}}/a_{\mathrm{NA}}] \\ &\simeq 54(\kappa/q_*A)[1-(T_{\mathrm{OH}}/T_*)^{5/2}] \ \ (\mathrm{MW}) \end{aligned} \tag{24c}$$

$$\beta_{\mathrm{th}*} = (\beta_e + \beta_i)_* = 1.15(m_*T_{10*})/q_*R_{\mathrm{o}}B_{\mathrm{o}} \tag{24d}$$

At ignition ($P_{\mathrm{aux}} = 0$), $m = m(T)$ and expressions for $m = 1$, $T(m = 1)$, and $T = 10$ keV, $m(T_{10} = 1)$ are easily obtained from Eq. (21). In both cases, β at ignition scales as

$$\beta_{\mathrm{ign}} \propto [q_*RB_{\mathrm{o}}(aB_{\mathrm{o}}^2/q_*)^{0.5}]^{-1} \tag{25}$$

Along the optimal path to ignition (and at ignition), the total fusion power produced is nearly the same in all devices (see Table II). However, the total (neutron plus alpha) wall loading varies widely, ranging from very low values in Super-JET to values approaching (or exceeding) reactor-like conditions in CITs. At maximum parameters ($n = n_{\mathrm{mu}}$, $\beta_{\mathrm{tot}} = \beta_{\mathrm{crit}}$), the power levels (and wall loadings in CITs) are very high. It should be noted, however, that with this optimistic confinement scaling, there is a large operating window (Figs 2 and 3), and ignition could have been achieved with lower B_0 and I (or these quantities could have been lowered after ignition is achieved) with correspondingly lower power levels.

Under the assumptions made here (i.e., nearly parabolic profiles, $Z_{\mathrm{eff}} \sim 1.5$, $q_{\mathrm{o}} \sim 0.95$, $\chi_e \sim \chi_i$, etc.), OH ignition is not possible in these devices. However, change in profiles, lower q_{o} and Z_{eff} values, higher density limits, etc., could alter the projections. In general, the optimal conditions needed for OH ignition are obtained from Eq. (2); these are $P_\alpha = P_{\mathrm{con}} = P_{\mathrm{rad}} = P_{\mathrm{OH}}$ (for $x = 1$, $y = 0$, $s = 3$). This corresponds to $P_{\mathrm{aux}*}(\mathrm{min}) = 0$, i.e., $T_{\mathrm{OH}} = T_*$, requiring a minimum aB_{o}^2/q_*. For $aB_{\mathrm{o}}^2/q_* > (aB_{\mathrm{o}}^2/q_*)_{\mathrm{min}}$, OH ignition is accessible within some density window.

The expression for the minimum value is

$$\begin{aligned} (aB_{\mathrm{o}}^2/q_*)_{\mathrm{min\text{-}OH}} &= a_{\mathrm{E}}a_B/\bar{a}_\alpha a_{\mathrm{OH}} \\ &\simeq 360(q_{\mathrm{o}}^2/q_*^2)[2\kappa/(1+\kappa_*^2)]^2 \end{aligned} \tag{26}$$

where $\bar{\gamma}_{\rm NC} \sim 2.5$ is assumed and $a_{\rm E} \simeq 6.5$ [Eq. (22)]. In terms of current, Eq. (26) can be rewritten as

$$(q_* IA)_{\text{min-OH}} \simeq 95\ \kappa q_{\rm o}(a/q_*)^{0.5} \tag{27}$$

Thus to achieve OH ignition, for example, if everything except $q_{\rm o}$ is kept constant, one needs

$$q_{\rm o} \leq \begin{cases} 0.65 & \text{in Super-JET} \\ 0.8 & \text{in CIT} \\ 0.8 & \text{in IGNITOR} \end{cases}$$

These low $q_{\rm o}$ values might be attainable if sawtoothing is suppressed. Alternatively, if the sawtooth activity limits $q_{\rm o}$ (~ 0.95), then OH ignition might be possible in these devices with further shaping of the plasma or with an increase in magnetic field. In the latter case, the magnetic fields and corresponding plasma currents needed for OH ignition are as follows:

$B_{\rm o} \geq 6$ T,	$I \geq 30$ MA	in Super-JET
≥ 12.5 T,	≥ 11 MA	in CIT, divertor
≥ 12.5 T,	≥ 12 MA	in CIT, limiter
≥ 16.5 T,	≥ 13.8 MA	in IGNITOR

An increase in elongation [see Eq. (26)] reduces the minimum $B_{\rm o}$ required for OH ignition, a result consistent with those obtained by Chu et al. [21].

4.2. Combined neoclassical ion and neo-Alcator electron scalings

For $\chi_e = f_{ex}\chi_{\rm NA}$ and $\chi_i = f_{ix}\chi_{\rm CH}$, Eq. (7) yields

$$\begin{aligned} F = -a_e T_{10} - (a_B + a_i) m^2 T_{10}^{1/2} + a_\alpha m^2 (T_{10}/0.75)^s \\ + a_{\rm OH} T_{10}^{-3/2} + a_{\rm aux} = 0 \end{aligned} \tag{28}$$

where a_B, a_α, $a_{\rm OH}$, and $a_{\rm aux}$ are given in Eq. (8), and $f_{\rm con}(m, T_{10}) = a_e T_{10} + a_i m^2 T_{10}^{1/2}$ with

$$a_e \simeq 3.43\ f_{ex}/(aB_{\rm o}^2/q_*) \equiv a_{e\rm o}/(aB_{\rm o}^2/q_*) \tag{29a}$$

$$\begin{aligned} a_i &\simeq 0.5/(n_{20}\tau_{Ei}) \equiv a_{i\rm o}/(aB_{\rm o}^2/q_*) \\ &\simeq 5.8 \times 10^{-2} f_{ix} K_2^* A^{3/2} (q_*/a)/[\kappa^2 (aB_{\rm o}^2/q_*)] \\ &\simeq 1.44 f_{ix} K_2^* [(1+\kappa_*^2)/2\kappa]^2 / A^{0.5} I^2 \end{aligned} \tag{29b}$$

Here $n_{20}\tau_{Ei}$ is given by Eq. (19b), where $A_i = 2.5$ and $Z_{\rm eff} \simeq 1.5$ is assumed. Equation (28) is similar to Eq. (21). For $A \sim 3 \pm 0.5$ and $q_* \sim 2$ (corresponding to $q_\psi \sim 2.5$–3.0), the ion neoclassical losses exceed the bremsstrahlung radiation if $aB_{\rm o}^2/q_* < 20 f_{ix}/a\kappa^2$ [or I (MA) $< 6 f_{ix}^{0.5}$].

The expressions for the scaling of parameters at various operating points are similar if $a_{\rm NA}$ is replaced with a_e and a_B is replaced with $a_B + a_i$ in Eqs (23) and (24). For example,

$$T_{10}({\rm OH}) \simeq (a_{\rm OH}/a_e)^{0.4} \quad , \quad T_{10*} = [(a_B + a_i)/\bar{a}_\alpha]^{0.4}$$

The optimal condition for OH ignition is determined from $P_\alpha = P_B + P_i = P_e = P_{\rm OH}$, which yields

$$(aB_{\rm o}^2/q_*)_{\rm min\text{-}OH} = \alpha_1[0.5 + 0.5(1 + 4\alpha_2/\alpha_1)^{0.5}] \tag{30}$$

where

$$\alpha_1 = a_{eo}a_B/\bar{a}_\alpha a_{\rm OH} \simeq 190(q_{\rm o}^2/q_*^2)[2\kappa/(1+\kappa_*^2)]^2 \; f_{ex}$$

$$\alpha_2 = a_{io}/a_B \simeq 0.97 f_{ix} K_2^* A^{3/2}(q_*/a\kappa^2)$$

[Here a_{eo} and a_{io} are defined in Eq. (29).]

Figure 4 shows, for $f_{ix} = 1$ and 3, the ignition contours and the extent of the ignition regimes in CIT, IGNITOR, and Super-JET. For $f_{ex} = 1$ and $f_{ix} = 1$, the IGNITOR ignites ohmically; however, OH ignition fails if $f_{ix} \geq 1.5$. The Super-JET comes very close to OH ignition with $f_{ix} \sim$ 1–2, because of the large current (ion neoclassical losses are nearly nonexistent). Figure 5 shows the auxiliary power contours for $f_{ix} = 3$. In CIT and IGNITOR the saddle point appears at $\langle n_* \rangle \sim (0.7\text{–}0.8)\langle n_{\rm mu} \rangle$ (i.e., $m_* \sim 0.7\text{–}0.8$), whereas in Super-JET $m_* \geq 1$. This is where ion conduction plus bremsstrahlung radiation losses (increasing with density) are comparable to electron conduction losses (decreasing with density). The minimum (steady-state) auxiliary power required to reach ignition is about 2–3 MW in IGNITOR and Super-JET and about 6 MW in CIT. In dynamic simulations, with finite startup time, the required power can be greater (or less) than these values, depending on the evolution of profiles and dynamics of the sawtooth activity [12,15]. The parameters corresponding to various operating points are summarized in Table III.

The $q_{\rm o}$ values needed for OH ignition (assuming sawtooth suppression) are:

	$q_{\rm o}$	
	$f_{ix} = 1$	$f_{ix} = 3$
IGNITOR	$\leq$1.0	$\leq$0.8
Super-JET	$\leq$0.9	$\leq$0.8
CIT	$\leq$0.85	$\leq$0.65

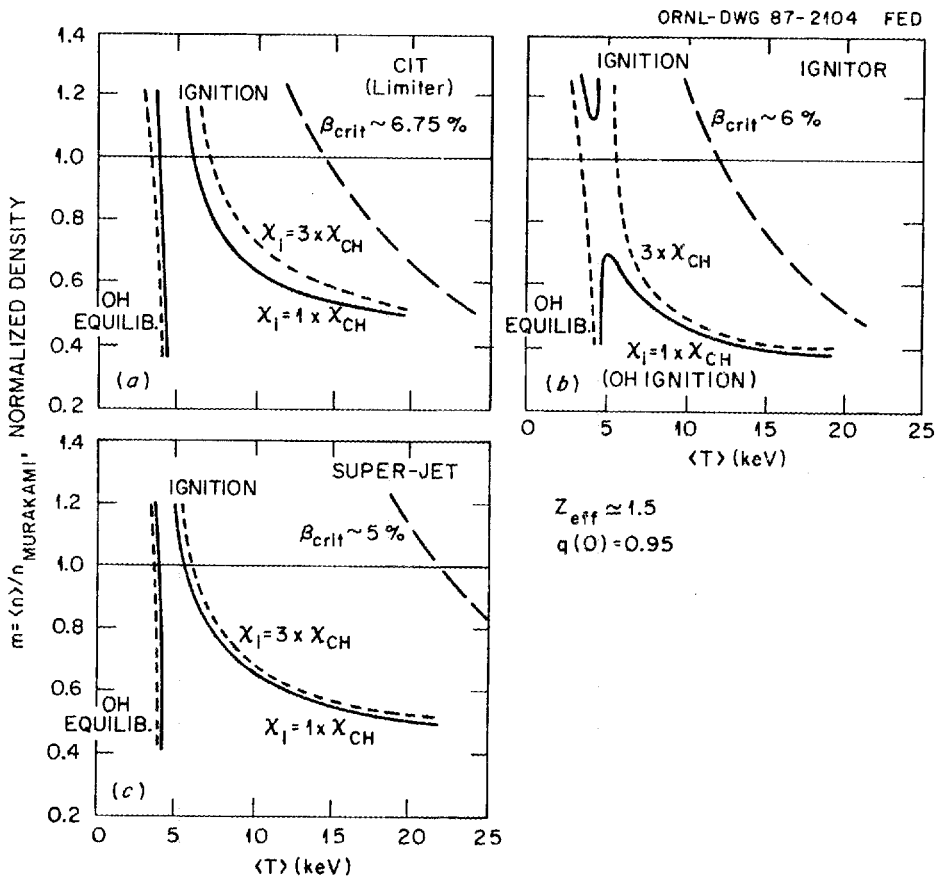

Fig. 4. Steady-state ignition and Ohmic equilibrium contours for (a) CIT, (b) IGNITOR, and (c) Super-JET. [$Z_{\rm eff} \simeq 1.5$ and $q(0) \simeq 0.95$.] Confinement model: $\chi_e = 1 \times \chi_{\rm NA}$, $\chi_i = f_{ix}\chi_{\rm CH}$, with $f_{ix} = 1$ and 3.

Alternatively, if $q(0) \sim 0.95$, the minimum OH ignition requirements are as follows:

	$f_{ix} = 1$		$f_{ix} = 3$	
	B_o (T)	I (MA)	B_o (T)	I (MA)
IGNITOR	"Ignited"		≥15	≥12.6
Super-JET	≥4.5	≥22.5	≥4.7	≥23.5
CIT, limiter	≥10.8	≥10.5	≥12.5	≥12
CIT, divertor	≥10.8	≥9.5	≥12.6	≥11

Note: f_{ix} is the ion neoclassical multiplier (anomaly).

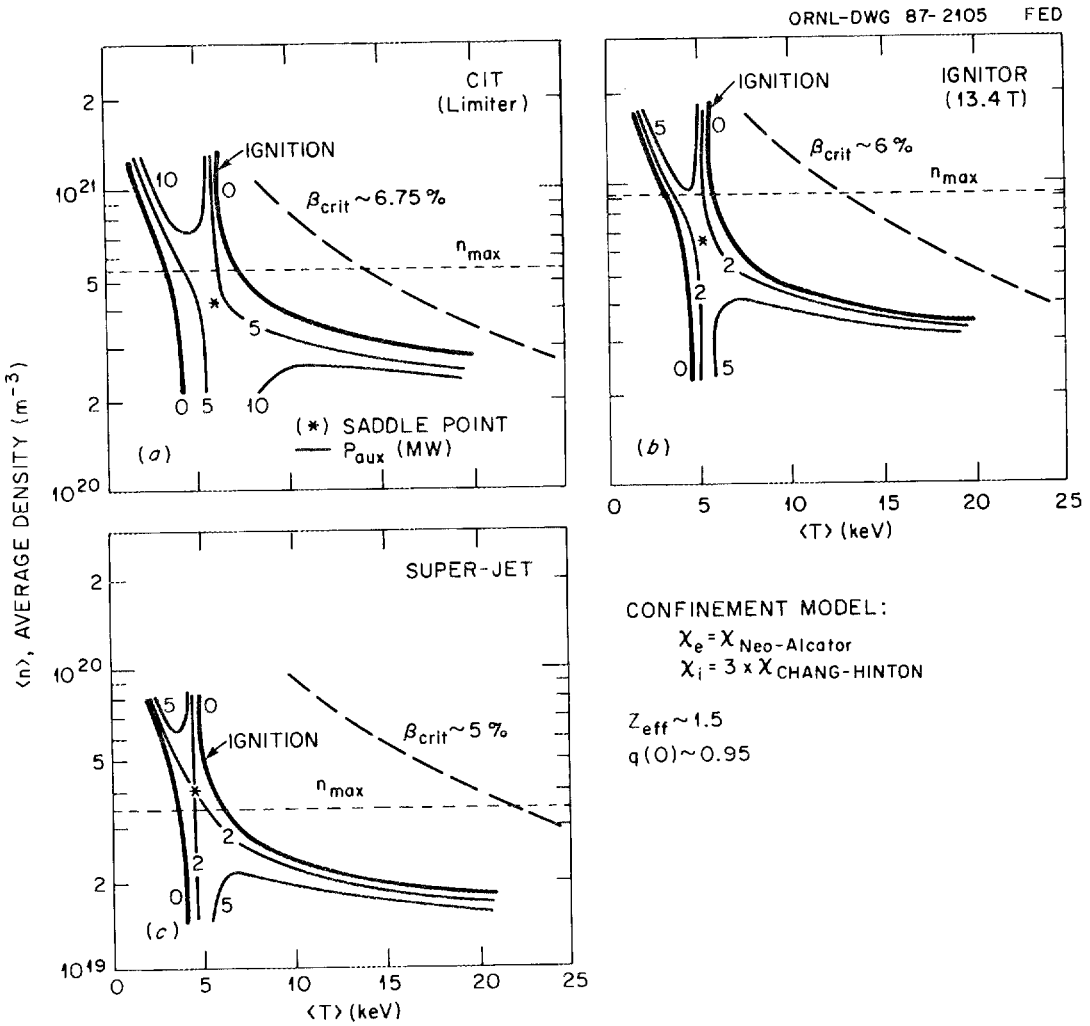

Fig. 5. Steady-state auxiliary power contours for (a) CIT, (b) IGNITOR, and (c) Super-JET. Confinement model: $\chi_e = \chi_{NA}$, $\chi_i = 3 \times \chi_{CH}$. [$Z_{eff} \simeq 1.5$ and $q(0) \simeq 0.95$.]

TABLE III. STEADY-STATE, VOLUME-AVERAGED PARAMETERS AT VARIOUS OPERATING POINTS FOR COMBINED NEOCLASSICAL ION AND NEO-ALCATOR ELECTRON SCALINGS: $\chi_e \simeq \chi_{NA}$ and $\chi_i \simeq f_{ix}\chi_{iCH}$ with $f_{ix} \sim 1$–3

	CIT-2		IGNITOR	Super-JET
	Limiter	Divertor	(13.4 T)	(2.5 × JET)
OH Equilibrium				
T_{OH} (keV)	4.5	4.5	4.8	4.1
Along optimal path (n_*, T_*)				
T_* (keV)	4.8–5.9	5.0–6.2	(5.3)[a] 4.6	4.3–4.5
n_* (10^{20}m^{-3})	5.8–4.3	5.5–3.9	(6.5)[a] 6.5	0.43–0.4
$m_* = n_*/\langle n_{mu}\rangle$	1.1–0.8	1.1–0.8	(0.7)[a] 0.7	1.3–1.2
β_{th*} (%)	2–1.8	2–1.7	(1.5)[a] 1.5	0.9–0.085
P_{fus*} (MW)	45–43	42–40	(50)[a] 50	41–40
L_{w*} (MW/m^2)	1.15–1.1	1.1–1.0	(1.85)[a] 1.85	0.035
Min P_{aux*} (MW)	1.6–5.7	1.8–6.0	0[a]–2.8	1–2
At ignition ($m = n/n_{mu} = 1$)				
T (keV)	6.1–7.2	6.4–7.9	5.3[a]-5.8	5.9–6.2
β_{th} (%)	2.3–2.7	2.3–2.8	1.5[a]–2.2	0.95–1.0
β_{pol}	0.34–0.4	0.4–0.5	0.2[a]–0.3	0.2–0.23
P_{fus} (MW)	75–120	75–125	50[a]–125	65–75
L_w (MW/m^2)	1.9–3.2	1.9–3.2	1.85[a]–4.7	0.05–0.06
At ignition (T = 10 keV)				
n (10^{20} m^{-3})	3.6–4.0	3.5–4.0	4.4–4.7	0.23
β_{th} (%)	2.5–2.8	2.6–2.9	1.9–2.0	1.1
β_{pol}	0.37–0.4	0.46–0.5	0.25	0.25
P_{fus} (MW)	110–135	105–135	115–130	105–110
L_w (MW/m^2)	2.8–3.5	2.7–3.5	4.3–4.8	0.09
At $n = n_{mu}$, $\beta_{tot} = \beta_{crit}$				
(Same as Table II)				

[a] *Note*: IGNITOR (13.4 T) ignites ohmically for $\chi_e \simeq \chi_{NA}$ and $\chi_i = 1 \times \chi_{iCH}$. Values given are at OH ignition ($n_* = 6.5 \times 10^{20}$ m^{-3}, $T_* = 5.3$ keV) for $f_{ix} = 1$. For $f_{ix} > 1.5$, OH ignition fails.

5. PERFORMANCE WITH AUXILIARY SCALINGS

5.1. Kaye-Goldston L-mode (H-mode) scaling

A generalized form of OH-auxiliary scaling is given by Eq. (20). Taking $\tau_{EOH} = \tau_{NA}$ and $\tau_{E\mathrm{aux}} = \tau_{KG}$ [Eq. (13)], Eq. (7) yields

$$F = -T_{10}\left(a_{NA}^2 + a_{KG}^2 m^{3.5} T_{10}^{2.76}\right)^{0.5} - a_B m^2 T_{10}^{1/2} + a_\alpha m^2 (T_{10}/0.75)^s + a_{OH} T_{10}^{-3/2} + a_{\mathrm{aux}} = 0 \tag{31}$$

where a_{NA} is given in Eq. (22), a_B, a_α, a_{OH}, and a_{aux} are given in Eq. (8), and $a_{KG} \propto (n_{20}\tau_{KG})^{-1}$, which is

$$a_{KG} = \frac{80}{(aB_o^2/q_*)^{1.5}} \left[\frac{a^{0.2} q_*^{1.7}}{(a/R_o)^{0.65}}\right] \frac{\kappa^{0.7}}{f_{LH}^{2.4}} \left(\frac{2}{1+\kappa_*^2}\right)^{2.95} \simeq 9.4 \times 10^3\ a^{1.65} \left[I^3 (R_o/a)^{2.3} f_{LH}^{2.4}\right]^{-1} \left(\kappa^{0.71} q_*^{0.24}\right) \tag{32}$$

As evidenced from Eq. (13) or (32), KG scaling is favorable in small-size, high-current devices. Ignition becomes easier if a given current can be generated in a smaller minor radius or if the current can be increased at a fixed size, both of which could be accomplished through shaping (κ) and/or higher field. The scaling also favors large aspect ratios. While both the CIT and IGNITOR ignite with KG L-mode ($f_{LH} = 1$) scaling, ignition in Super-JET would require either $I \sim 29$ MA or an L-mode enhancement factor $f_{LH} > 1.7$. A simple estimate of the relationship between size, aspect ratio, and required current for L-mode ignition is

$$I > 33 a^{0.5} A^{-0.75} \tag{33}$$

For a "CIT-class" device with $a \sim 0.4$–0.5 m and $A \sim 3 \pm 0.5$, the required current is about 10 ∓ 1 MA. (For Super-JET, $a \sim 3$ m and $A \sim 2.5$, requiring $I \sim 29$ MA.) In terms of aB_o^2/q_*, the ignition requirement is roughly given by

$$aB_o^2/q_* \simeq 43.5\ q_* A^{0.5} [2/(1+\kappa_*^2)]^2 \tag{34}$$

Ignition contours ($P_{\mathrm{aux}} = 0$) for various values of aB_o^2/q_* are shown in Fig. 6 for L-mode operation of a "CIT-class" tokamak with $A \sim 2.8 \pm 0.2$, $\kappa \sim 1.8$, $\delta \sim 0.2$, $q_* \sim 2$, and $a \sim 0.4$–0.5 m. The beta limits ($\beta_{tot} = \beta_{crit}$) corresponding to 8, 10, and 12 MA are also shown. For the assumptions of this geometry (κ, A), the devices with $aB_o^2/q_* < 27$ reach their beta and density limits before ignition is achieved. If the density limit is considerably higher than indicated by the Murakami limit (if, for example, the Greenwald limit [22] applies, see Table I), then ignition may become possible for lower values of aB_o^2/q_*. An increase in elongation [see Eqs (32) and (34)] further reduces this limit. Figure 7 shows the maximum attainable ignition margin versus aB_o^2/q_* for two plasma elongations. Considering Murakami density ($m < 1$) and Troyon-Gruber beta ($\beta < \beta_{crit} = 3I/aB_o$ %) limits, the results of

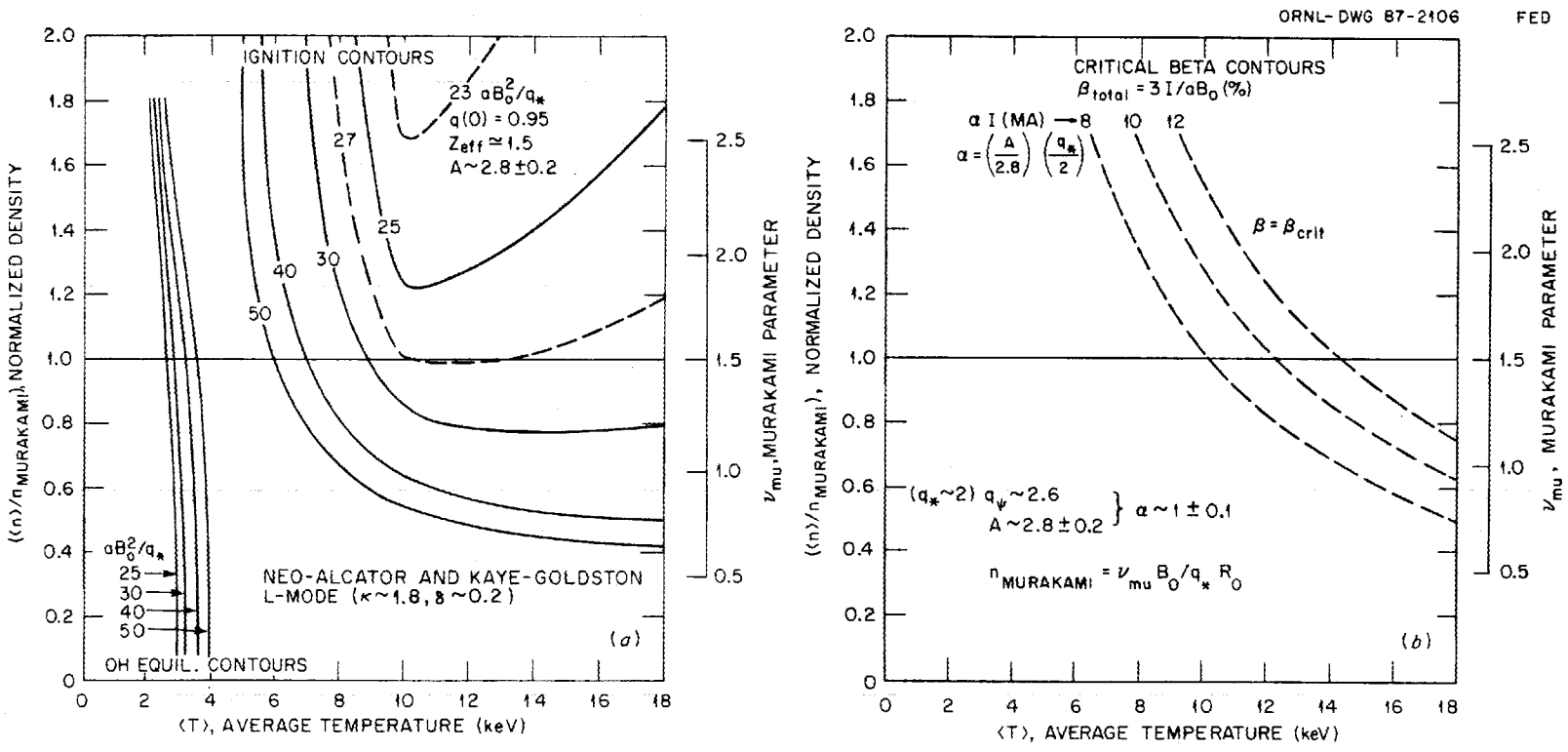

Fig. 6. (a) Steady-state ignition contours for various values of aB_o^2/q_* for combined neo-Alcator (NA) and Kaye-Goldston (KG) L-mode scaling. For a given aB_o^2/q_*, $P_{aux} = 0$ on the designated curves. $P_{aux} > 0$ is required to bridge the gap between OH equilibrium and ignition branches. Compact tokamak geometry is assumed: $a \sim 0.4$–0.5 m, $A \sim 2.8 \pm 0.2$, $\kappa \sim 1.8$, $\delta \sim 0.2$, $q_* \sim 2$. [$Z_{eff} \simeq 1.5$ and $q(0) \simeq 0.95$.] Confinement model: $1/\tau_E^2 = 1/\tau_{NA}^2 + 1/\tau_{KG}^2$.
(b) $\beta = \beta_{crit}$ contours for $\alpha I = 8$, 10, and 12; $\alpha = (A/2.8)(q_*/2)$. [The fast alpha contribution to total beta is included.]

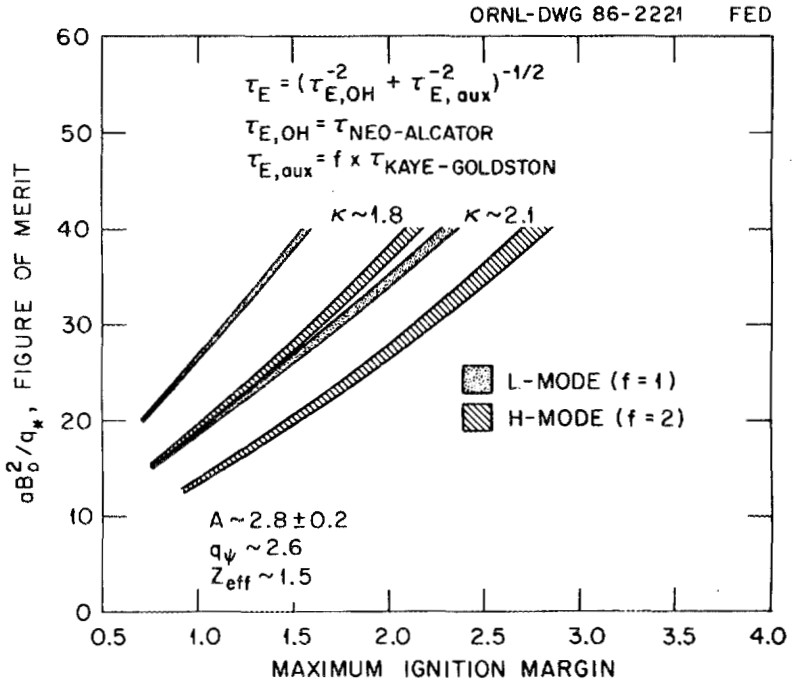

Fig. 7. Maximum attainable ignition margin vs aB_o^2/q_* for (a) Ohmic-like and (b) Ohmic + auxiliary (Kaye-Goldston) scalings.

Figs 6 and 7 show that "CIT-class" devices with $aB_o^2/q_* \sim 25$–30 ($B_oI \sim 100$–120), $\kappa \sim 1.8$, and $A \simeq 2.8 \pm 0.2$ (corresponding to a set of device parameters $a \sim 0.4$–0.5 m, $R_o \sim 1.1$–1.5 m, $B_o \sim 10$–12 T, $I \sim 10$–11 MA) should be ignitable with a small ignition window under the conservative KG L-mode scaling. For $\kappa \sim 2$, $aB_o^2/q_* \sim 20$ is needed for ignition.

Note that the projected favorable results for plasmas with strong shaping are subject to experimental verification [to investigate whether the plasma shaping (large κ) really helps to improve confinement through increased plasma current at fixed safety factor] and should be treated with caution. This is because the experimental data [16] from which these scalings are deduced are typically limited to a range at which $\kappa \leq 1.8$. Also important is the linear scaling of the beta limit with plasma current. Although for many tokamaks ($\kappa \leq 1.8$, $\delta \leq 0.5$, $A \sim 3$), the Troyon-Gruber formula ($\beta_{crit} \sim C_\beta I/aB_o$ with $C_\beta \sim 2.5$–3.5) gives a good description of the operating limits [16], the scaling of C_β with q_* (q_ψ) and geometry (κ, δ, A) has not yet been clearly established.

Assuming $\tau_E = \tau_{E\text{aux}}$ or $\tau_E = (\tau_{E\text{OH}}^{-2} + \tau_{E\text{aux}}^{-2})^{-1/2}$ with $\tau_{E\text{OH}} = \tau_{\text{NA}}$ and $\tau_{E\text{aux}} = \tau_{\text{KG}}$, ignition requirements for CITs and Super-JET are as follows:

	$\tau_E = \tau_{KG}$	$\tau_E = (\tau_{NA}^{-2} + \tau_{KG}^{-2})^{-1/2}$
IGNITOR	Ignited	Ignited
CIT, limiter	Ignited	~Ignited
CIT, divertor	Ignited	$f_{LH} \geq 1.1$
Super-JET	$f_{LH} \geq 1.7$	$f_{LH} \geq 1.9$

Note: f_{LH} is the needed enhancement factor over L-mode.

5.2. Goldston L-mode (H-mode) scaling

The power balance equation for the Goldston scaling is similar to Eq. (31), except for the first term $f_{con}(m,\ T_{10})$, which is given by

$$f_{con}(m,\ T_{10}) = T_{10}\left(a_{NA}^2 + a_G^2 m^4 T_{10}^2\right)^{0.5} \tag{35}$$

where

$$a_G \simeq 3.95 \times 10^3\ a^{0.24}/(I^2 A^{2.5} f_{LH}^2) \tag{36}$$

Here Eq. (14b) is used. The current and $A = R_o/a$ are the only strong scaling parameters in this scaling. The minor radius dependence is weak. None of the examples given in Table I ignite with Goldston L-mode. Enhancement over L-mode (i.e., H-mode) should provide ignition. The needed enhancement factors [assuming $\tau_E = \tau_{Eaux} = \tau_G$ or $\tau_E = (\tau_{EOH}^{-2} + \tau_{Eaux}^{-2})^{-1/2}$ with $\tau_{EOH} = \tau_{NA}$ and $\tau_{Eaux} = \tau_G$] are as follows:

	f_{LH}	
	$\tau_E = \tau_G$	$\tau_E = (\tau_{NA}^{-2} + \tau_G^{-2})^{-1/2}$
Super-JET	$\geq$1.65	$\geq$1.9
CIT, divertor	$\geq$2.0	$\geq$2.4
CIT, limiter	$\geq$2.0	$\geq$2.2
IGNITOR	$\geq$2.1	$\geq$2.2

Note: f_{LH} is the needed enhancement factor over L-mode.

In general, ignition with Goldston scaling requires (assuming $\tau_E \simeq \tau_G$)

$$IA^{1.25} \geq 90a^{0.12}/f_{LH} \tag{37}$$

For compact CIT-like devices ($a \sim$ 0.4–0.5 m), the required plasma current for ignition is

L-mode: $I \simeq 20 \pm 5.0$ MA for $A \sim 3 \mp 0.5$
H-mode: $I \simeq 10 \pm 2.5$ MA for $A \sim 3 \mp 0.5$

For Super-JET-like devices ($a \sim$ 2–3 m) the required plasma current for ignition is

L-mode: $I \simeq 25 \pm 6$ MA for $A \sim 3 \mp 0.5$
H-mode: $I \simeq 13 \pm 3$ MA for $A \sim 3 \mp 0.5$

5.3. Mirnov-like scaling

Taking $\tau_{EOH} = \tau_{NA}$ and $\tau_{E\text{aux}} = \tau_{MI}$,

$$f_{\text{con}}(m,\ T_{10}) \simeq T_{10}(a_{NA}^2 + a_{MI}^2 m^2)^{0.5} \tag{38a}$$

where

$$\begin{aligned} a_{MI} &= K_L(R_o/L)q_*/B_o I f_{LH} \\ &= 0.2K_L(R_o/L)q_* A[2/(1+\kappa_*^2)]/(aB_o^2/q_*)f_{LH} \end{aligned} \tag{38b}$$

For $L = a$, $K_L = K_a \simeq 4.5$–12.5 [see Eq. (15)], and for $L = R_o$, $K_L = K_{R_o} \simeq 12.5$–$33$ [see Eq. (16)]. As a representative case, choosing

$$\tau_{MI} \simeq 0.075 a I \kappa^{0.5}(A_i/2.5)^{0.5} \tag{39}$$

yields (for $A_i = 2.5$)

$$\begin{aligned} a_{MI} &\simeq 8.9 q_* \kappa^{0.5} A/B_o I f_{LH} \\ &\simeq 1.78 q_* A^2[2\kappa^{0.5}/(1+\kappa_*^2)]/(aB_o^2/q_*)f_{LH} \end{aligned} \tag{40}$$

The power balance equation is similar to Eqs (31) and (35), except for the first term $f_{\text{con}}(m,\ T_{10})$, which is given by Eq. (38). The current, field, and aspect ratio are equally strong scaling parameters. (For $L = R_o$, $\tau_{MI} \sim R_o I$, the aspect ratio dependence is not as strong as for $L = a$.) The ignition contours for various values of aB_o^2/q_* are shown in Fig. 8 for L-mode operation ($f_{LH} = 1$) of tokamaks having $A \sim 3$, $\kappa \sim 1.6$–1.8, $\delta \sim 0.3$–0.1, $q_* \sim 2$, $Z_{\text{eff}} \sim 1.5$, and $q(0) \sim 0.95$. Critical beta contours for various plasma currents are shown in Fig. 6(b). For nominal density ($m \leq 1$) and beta ($\beta \leq \beta_{\text{crit}}$) limits, the results from Figs 8 and 6(b) indicate that devices with $aB_o^2/q_* \sim 20$–25, $I \sim 10$–12 MA, and $A \sim 3 \pm 0.5$ are ignitable with the L-mode (Mirnov-like) scaling given by Eq. (39). Both of the CITs and the Super-JET ignite (or require only a small enhancement factor) with this L-mode scaling. Typically, ignition is easier to attain for scalings in the form of Eq. (39) [or Eqs (15) and (16)] than for the power law scalings of Goldston or Kaye-Goldston.

Assuming $\tau_E = \tau_{E\text{aux}}$ or $\tau_E = (\tau_{EOH}^{-2} + \tau_{E\text{aux}}^{-2})^{-1/2}$ with $\tau_{EOH} = \tau_{NA}$ and $\tau_{E\text{aux}} = \tau_{MI}$, the ignition requirements are as follows:

	$\tau_E = \tau_{MI}$	$\tau_E = (\tau_{NA}^{-2} + \tau_{MI}^{-2})^{-1/2}$
Super-JET	~ Ignited	$f_{LH} \geq 1.25$
CIT, limiter	Ignited	~ Ignited
CIT, divertor	~ Ignited	$f_{LH} \geq 1.35$
IGNITOR	Ignited	Ignited

Note: f_{LH} is the needed enhancement factor over L-mode.

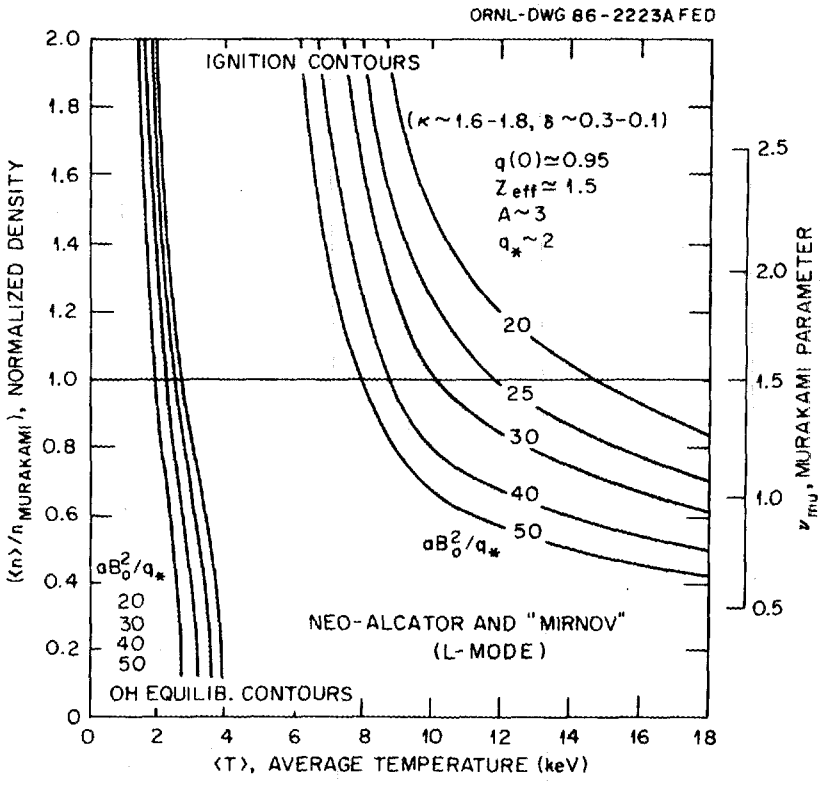

Fig. 8. Steady-state ignition contours for various values of aB_o^2/q_* for combined neo-Alcator (NA) and Mirnov-like (MI) L-mode scalings.

5.4. T-10/T-11 scaling

The T-10/T-11, or Mukhovatov-Merezhkin, scaling for τ_{Ee} ($= \tau_{\rm MM}$) is given by Eq. (17), which contains a linear density and a cubic size dependence. The reduction in confinement is proportional to $T^{-1/2}$. Given τ_{Ee}, τ_E can be estimated in one of two ways: (1) $\tau_E = f_\tau \tau_{Ee} = f_\tau \tau_{\rm MM}$ with $f_\tau \simeq$ 1–2 or (2) $\tau_{Ee} = \tau_{\rm MM}(\chi_e = \chi_{\rm MM})$ and $\tau_{Ei} = \tau_{\rm CH}/f_{ix}(\chi_i = f_{ix}\chi_{\rm CH})$.

1. First consider $\tau_E = f_\tau \tau_{Ee}$. With this assumption, Eq. (7) becomes

$$F = -a_{E\rm MM}T_{10}^{3/2} - a_B m^2 T_{10}^{1/2} + a_\alpha m^2 (T_{10}/0.75)^s + a_{\rm OH}T_{10}^{-3/2} + a_{\rm aux} = 0 \tag{41}$$

where

$$a_{E\rm MM} = 68/[(aB_o^2/q_*)A^{0.75}f_\tau] \equiv a_{E\rm M}/(aB_o^2/q_*) \tag{42}$$

Equation (41) can be solved analytically with $m = f(T,\ aB_o^2/q_*)$ for a given geometry (A, κ). The minimum value of aB_o^2/q_* needed for ignition [subject to density

($m < 1$) and beta ($\beta < \beta_{\rm crit}$) limits] depends on the aspect ratio and plasma current, which can be simplified as

$$aB_o^2/q_* \gtrsim (60/f_\tau)(3/A)^{1.25}(10/I)^{0.5}(1/m)^{1.5} \tag{43}$$

For example, for $m \leq 1$ and $A \simeq 3$, $aB_o^2/q_* \gtrsim 30$ (60) for $f_\tau \simeq 2$ (1), requiring $I \sim 10$ MA. If the density limit is higher (i.e., $m > 1$) than indicated by the Murakami limit, ignition may become possible for lower values of aB_o^2/q_*, scaling roughly as $1/m^{1.5}$.

With this scaling, under nominal assumptions ($m \leq 1$, $f_\tau \sim 1$–2, $\beta < \beta_{\rm crit}$, etc.), neither CITs nor Super-JET ignites. When conditions are relaxed, the ignition requirements are as follows:

	m	
	$f_\tau \simeq 1$	$f_\tau \simeq 2$
IGNITOR	$\geq$1.6	Ignited
CIT, limiter	$\geq$2.0	$\geq$1.25
CIT, divertor	$\geq$2.1	$\geq$1.3
Super-JET	$\geq$3.1	$\geq$2.0

Note: m is the needed increase over the Murakami density limit [$m = n/n_{\rm max} = n_{20}/(1.5B_o/q_*R_o)$].

The optimal path to ignition (m_*, T_*) is determined from Eq. (2), where $x = 1$, $y = -1/2$, and $s = 3$:

$$T_{10}({\rm OH}) = (a_{\rm OH}/a_{EMM})^{1/3} \tag{44a}$$

$$T_{10*} = (a_B/\bar{a}_\alpha)^{0.4} \simeq 0.42 \tag{44b}$$

$$m_*T_{10*} = [0.6(a_{\rm OH}/a_B) + 0.6(a_B/\bar{a}_\alpha)^{0.2}(a_{EMM}/\bar{a}_\alpha)]^{0.5} \tag{44c}$$

$$\begin{aligned} P_{{\rm aux}*}({\rm min}) &= P_{\rm con} - P_{\rm OH} \quad {\rm at} \quad (m_*,\ T_*) \\ &= (360/f_\tau)(\kappa/q_*A^{1.75})[1 - (T_{\rm OH}/T_*)^3] \quad ({\rm MW}) \end{aligned} \tag{44d}$$

$$\beta_{{\rm th}*} = (\beta_e + \beta_i)_* = 1.15(m_*T_{10*})/q_*R_oB_o \tag{44e}$$

The optimal OH ignition condition is $P_\alpha = P_{\rm rad} = 1.2P_{\rm con} = 1.2P_{\rm OH}$, which corresponds to $P_{{\rm aux}*}({\rm min}) = 0$, i.e., $T_{\rm OH} = T_*$, requiring a minimum aB_o^2/q_*,

$$\begin{aligned} (aB_o^2/q_*)_{\text{min-OH}} &\simeq (a_{EM}/a_{\rm OH})(a_B/\bar{a}_\alpha)^{1.2} \\ &\simeq (2450/f_\tau A^{0.75})(q_o^2/q_*^2)[2\kappa/(1+\kappa_*^2)]^2 \end{aligned} \tag{45}$$

In terms of current, Eq. (45) can be rewritten as

$$(q_* I A^{1.38})_{\text{min-OH}} \simeq (248/f_r^{0.5})\kappa q_o (a/q_*)^{0.5} \tag{46}$$

To achieve OH ignition in CITs and Super-JET, one needs

	Fixed I, B	$q(0) \simeq 0.95$ (fixed)	
	q_o	I (MA)	B_o (T)
Super-JET	$\leq$0.5	$\geq$39	$\geq$7.8
CIT, limiter	$\leq$0.7	$\geq$14	$\geq$14.5
CIT, divertor	$\leq$0.7	$\geq$12.5	$\geq$14.3
IGNITOR	$\leq$0.6	$\geq$17.5	$\geq$21

2. Next consider $\tau_{Ee} = \tau_{\text{MM}}$ and $\tau_{Ei} = \tau_{\text{CH}}/f_{ix}$. The power balance equation is similar to Eq. (41), except that the conduction term is replaced with

$$f_{\text{con}}(m,\ T) = a_{\text{emm}} T_{10}^{3/2} + a_i m^2 T_{10}^{1/2} \tag{47a}$$

where a_i is given by Eq. (29b) and

$$\begin{aligned} a_{\text{emm}} &\equiv a_{em}/(aB_o^2/q_*) \\ &= 36/A^{0.75}(aB_o^2/q_*) \end{aligned} \tag{47b}$$

The expressions for the scaling of parameters at various operating points are similar if the following substitutions are made: a_{EMM} (a_{EM}) is replaced with a_{emm} (a_{em}), and a_B is replaced with $a_B + a_i$ in Eqs (41) and (44). The optimal OH ignition condition is determined from $P_\alpha = P_{\text{rad}} + P_i = 1.2P_e = 1.2P_{\text{OH}}$.

6. DISCUSSION

A simple analytic model, which incorporates profile effects, is presented, treating the question of relative merits of size, field, and current on the ignition capability of tokamaks. Despite the idealized and simple nature of the (0-D) model, the analytic results obtained and scaling relationships derived agree qualitatively and quantitatively with more sophisticated transport code (1 1/2-D WHIST) calculations. (Direct comparisons between the global and 1 1/2-D WHIST transport calculations are given in Ref. [15] for a small subset of the confinement models considered here.) The global studies reported here have particular value because of the ease of calculating and presenting results and folding them into an evaluation of optimal sets of machine and physics performance parameters under various physics assumptions and constraints (χ_e and χ_i or τ_E, n_{max}, β_{crit}, q_*, etc.).

The uncertainties in present-day understanding of confinement and the existence of a large number of empirical scaling laws make it difficult to determine a precise physical quantity that identifies ignition potential. For a wide range of confinement models considered in this paper, several "figure-of-merit" parameters are found to

give a good indication of the relative performance of devices as measured by the ease with which ignition can be achieved and the extent (in density and temperature space) of the ignition regime (see Fig. 1). With the plasma density regime identified in terms of $m \sim n/n_{\max} < 1$ ($n_{\max} \sim B_o/R_o \sim J$) and the temperature regime in terms of $\beta_{\text{crit}} \sim I/aB_o$ ($T_{\max} \sim T_{\text{crit}} \sim I$), for many of the scalings considered, the figure-of-merit parameters that identify the ignition capability of the devices are $X_m = aB_o^2/q_* \propto B_o I$ and I. The specific form of geometry (A, κ) dependence varies among the scaling laws. The confinement scalings selected cover the range of possibilities ("optimistic," "middle-of-the-road," and "pessimistic"), thus providing lower and upper bounds on the figure-of-merit parameters.

For a given confinement scaling law, the minimum requirements for ignition are established, and generic ignition contours (in m-T space) for various values of aB_o^2/q_* are presented. Expressions for the optimal path to ignition (saddle point—n_*, T_*) and the minimum conditions needed for ohmic ignition are derived analytically. As an illustration, the results are applied to CIT [5], IGNITOR [4], and Super-JET [8]. The figure-of-merit parameters corresponding to these devices are summarized in Table I; all of them are variations of aB_o^2/q_* and IA except B_o/R_o. The importance of B_o/R_o has long been stressed (e.g., in Refs [1] and [4]).

As pointed out earlier, determination of the precise physical quantity required for ignition depends in part on the selected confinement model. However, the results of calculations indicate common figures of merit for a wide range of confinement models. Specific findings are as follows:

1. a typical L-mode ignition should be accessible in devices with $aB_o^2/q_* \sim 25 \pm 5$ (or equivalently, $B_o I \sim 110 \pm 20$), $\kappa \sim 1.8$–2, and $A \sim 2.8 \pm 0.2$;
2. the possibility of an H-mode (although precise scaling is less known) and/or increased plasma elongation κ (although the existing data base is limited) improves the prospects for ignition and lowers the required values of aB_o^2/q_* (or $B_o I$) by as much as 50%; and
3. prospects for ohmic ignition exist for devices with $aB_o^2/q_* \sim (40$–$50)q_o^2$, $\kappa \sim 1.8$–2.0 under favorable (nonsaturated) ohmic-like confinement scalings. Typically, $aB_o^2/q_* \sim 80 \pm 10$ would be required for L-mode scalings. Note that, in designs with very high fields ($B_o > 15$ T), synchrotron radiation (which is not covered in this study) could play an important role.

ACKNOWLEDGMENT

The topic was suggested to the author by H. Furth. Discussions with J. Sheffield and the advice and encouragement of H. Furth are gratefully acknowledged. The author is indepted to P. Rebut, S. Kaye, D. Cohn, W. Houlberg, M. Saltmarsh, T. K. Fowler, F. Engelmann, and B. Coppi for valuable comments and suggestions on the manuscript.

REFERENCES

1. COPPI, B., *Comments Plasma Phys. Controlled Fusion* **3** (1977) 47; Massachusetts Institute of Technology, R.L.E. Report PRR-75/18 (1975).
2. COHN, D. R., PARKER, R. R., JASSBY, D. L., Nucl. Fusion **16** (1976) 31.
3. COHN, D. R., WILLIAMS, J. E. C., BROMBERG, L., KREISCHER, K., MONTGOMERY, D. B., PARKER, R. R., in Fusion Reactor Design Concepts (Proc. 2nd IAEA Workshop, Madison, 1977), IAEA, Vienna (1978) 113.
4. COPPI, B., LANZAVECCHIA, L., IGNITOR DESIGN GROUP, Compact Ignition Experiments: Physics and Design Issues, Massachusetts Institute of Technology, R.L.E. Report PTP-86/12 (1986); to be published in Comments Plasma Phys. Controlled Fusion.
5. SCHMIDT, J., BATEMAN, G., BLACKFIELD, D. BROMBER, L., BUSHNELL, C., CITROLO, J., COHN, D., COLESTOCK, P., FLANAGAN, C., GREENWALD, M. HOULBERG, W., HUGHES, M., IGNAT, D., IZZO, R., JARDIN, S., KERBEL, G., KU, L. P., KUO-PETRAVIC, G., LIPSCHULTZ, B., MONTGOMERY, B., PARKER, R., PAULSON, C., PENG, Y-K. M., PETRAVIC, M., PHILLIPS, C. K., PHILLIPS, M., POMPHREY, N., POST, D., PUHN, F., SHANNON, T., SHEFFIELD, J., SIGMAR, D., STRICKLER, D., SWAIN, D., SWANSON, G., THOME, R., TODD, A., UCKAN, N., WHITE, R., WOLFE, S. YOUNG, K., in Plasma Physics and Controlled Nuclear Fusion Research 1986 (Proc. 11th Int. Conf. Kyoto, 1986), IAEA, Vienna (1987).
6. DeMARCO, F., PIERONI, L., SANTINI, F., SEGRE, S. E., *Nucl. Fusion* **26** (1986) 1193.
7. See "Near Term Tokamak Reactors" papers in Fusion Reactor Design IV (Proc. 4th IAEA Workshop Yalta, 1986), IAEA, Vienna (1987); also ABDOU, M. A., BERTOLINI, E., HANCOX, R., HOGAN, W. J., KOSTENKO, A. I., KULCINSKI, G. L., MILLER, R. L., ORLOV, V. V., RAU, F., SVIATOSLAVSKY, I. N., KUPITZ, J., *Nucl. Fusion* **26** (1976) 1377.
8. REBUT, P. H., JET TEAM, in Plasma Physics and Controlled Nuclear Fusion Research 1986 (Proc. 11th Int. Conf. Kyoto, 1986), IAEA, Vienna (1987).
9. COHN, D. R., BROMBERG, L., LeCLAIRE, R. J., POTOK, R. E., JASSBY, D. L., *Fusion Technol.* **10** (1986) 1111.
10. CARRERA, R., MONTALVO, E., ROSENBLUTH, M. N., Bull. Am. Phys. Soc. **31** (1986) 1565.
11. CORDEY, J. G., FIELD, J. J., ROBERTSON, I. L., in Physics of Plasmas in Thermonuclear Regimes (Proc. Varenna Workshop, 1979), U.S. Department of Energy Report CONF-790866 (1981) 89.
12. HOULBERG, W. A., ATTENBERGER, S. E., HIVELY, L. M., *Nucl. Fusion* **22** (1976) 935.
13. MURAKAMI, M., CALLEN, J. D., BERRY, L. A., *Nucl. Fusion* **16** (1976) 347.
14. TROYON, F., GRUBER, R., SAURENMANN, H., SEMENZATO, S., SUCCI, S., Plasma Phys. Controlled Fusion **26** (1984) 209; TROYON, F., GRUBER, R., Phys. Lett. A **110** (1985) 29.
15. UCKAN., N. A., SHEFFIELD, J., in *Tokamak Startup* (Ed. H. Knoepfel), Plenum Press (1986) 45; UCKAN, N. A., HOULBERG, W. A., SHEFFIELD,

J., in Proc. 11th Symp. Fusion Engineering (Austin, Texas, 1985) Vol. 1 (1986) 401.

16. See papers (and references therein) in *25 Years of Nuclear Fusion, Anniversary Issue,* Nucl. Fusion **25** (1985) 1011–1194; see also tokamak papers in Plasma Physics and Controlled Nuclear Fusion Research 1986 (Proc. 11th Int. Conf. Kyoto, 1986), IAEA, Vienna (1987).
17. KAYE, S. M., GOLDSTON, R. J., Nucl. Fusion **25** (1985) 65; KAYE, S. M., Phys. Fluids, **28**, (1985) 2327.
18. GOLDSTON, R. J., Plasma Phys. Controlled Fusion **26** (1984) 87.
19. See STRELKOV, V. S., Nucl. Fusion **25** (1985) 1189.
20. CHANG, C. S., HINTON, F. L., Phys. Fluids **25** (1982) 1493; **29** (1986) 3314.
21. CHU, M. S., HARVEY, R. W., POLITZER, P. A., YAMAGISHI, T., Nucl Fusion **25** (1985) 835.
22. GREENWALD, M., BESEN, M., CAMACHO, F., FIERO, C., FOORD, M., GANDY, R., COMEZ, C., GRANETZ, R. GWINN, D., KNOLWTON, S., LaBOMBARD, B., LIPSHCULTZ, B., MANNING, H., MARMAR, E., McCOOL, S., PARKER, J., PARKER, R., PETRSSO, R., PRIBYL, P., RICE, J., SIGMAR, D., TAKASE, T., TERRY. J., WATTERSON, R., WOLFE, S., in Plasma Physics and Controlled Nuclear Fusion Research 1986 (Proc. 11th Int. Conf. Kyoto, 1986), IAEA, Vienna (1987).

ORNL/TM-10365
Dist. Category UC-20 a,d,f,g

INTERNAL DISTRIBUTION

1. D. L. Akers
2. L. A. Berry
3. B. A. Carreras
4. R. A. Dory
5. J. L. Dunlap
6. J. D. Galambos
7. W. A. Houlberg
8. H. C. Howe
9. M. Murakami
10. W. D. Nelson
11. S. L. Painter
12. Y-K. M. Peng
13. R. L. Reid
14. M. J. Saltmarsh
15. T. E. Shannon
16. J. Sheffield
17. C. A. Smith
18–22. N. A. Uckan
23. T. Uckan
24–25. Laboratory Records Department
26. Laboratory Records, ORNL-RC
27. Document Reference Section
28. Central Research Library
29. Fusion Energy Division Library
30–31. Fusion Energy Division Publications Office
32. ORNL Patent Office

EXTERNAL DISTRIBUTION

33. M. A. Abdou, School of Engineering and Applied Science, 6288 Boelter Hall, University of California, Los Angeles, CA 90024
34. C. C. Baker, Argonne National Laboratory, 9700 South Cass Avenue, Argonne, IL 60439
35. C. Bolton, Office of Fusion Energy, Office of Energy Research, Germantown ER-55, U.S. Department of Energy, Washington, DC 20545
36. D. R. Cohn, 167 Albany St., NW 16-140, Massachusetts Institute of Technology, Cambridge, MA 02139
37. R. W. Conn, Fusion Engineering and Physics Program, 6291 Boelter Hall, University of California, Los Angeles, CA 90024
38. B. Coppi, 77 Massachusetts Avenue, 26-217, Massachusetts Institute of Technology, Cambridge, MA 02139
39. R. C. Davidson, 77 Massachusetts Avenue, Massachusetts Institute of Technology, Cambridge, MA 02139
40. N. A. Davies, Office of Fusion Energy, Office of Energy Research, ER-55 Germantown, U.S. Department of Energy, Washington, DC 20545
41. S. O. Dean, Director, Power Associates, Inc., 2 Professional Drive, Suite 249, Gaithersburg, MD 20760

42. S. A. Eckstrand, Office of Fusion Energy, Office of Energy Research, ER-55 Germantown, U.S. Department of Energy, Washington, DC 20545
43. G. A. Eliseev, I. V. Kurchatov Institute of Atomic Energy, P.O. Box 3402, 123182 Moscow, U.S.S.R.
44. A. J. Favale, Grumman Aerospace Corporation, MS-A0126, P.O. Box 31, Bethpage, NY 11714
45. H. K. Forsen, Bechtel Group, Inc., Research & Engineering, P.O. Box 3965, San Francisco, CA 94119
46. T. K. Fowler, Lawrence Livermore National Laboratory, P.O. Box 5511 (L-640), Livermore, CA 94550
47. H. P. Furth, Princeton Plasma Physics Laboratory, P.O. Box 451, Princeton, NJ 08544
48. J. R. Gilleland, GA Technologies, Inc., P.O. Box 85608, San Diego, CA 92138
49. V. A. Glukhikh, Scientific-Research Institute of Electro-Physical
50. R. J. Goldston, Princeton Plasma Physics Laboratory, P.O. Box 451, Princeton, NJ 08544
51. R. W. Gould, Department of Applied Physics, California Institute of Technology, Pasadena, CA 91125
52. C. D. Henning, Lawrence Livermore National Laboratory, P.O. Box 5511 (L-644), Livermore, CA 94550
53. T. R. James, Office of Fusion Energy, Office of Energy Research, ER-55 Germantown, U.S. Department of Energy, Washington, DC 20545
54. R. A. Krakowsi, CTR-12, Mail Stop 641, Los Alamos National Laboratory, P.O. Box 1663, Los Alamos, NM 87545
55. G. L. Kulcinski, Department of Nuclear Engineering, University of Wisconsin, Engineering Research Building, Room 439, 1500 Johnson Drive, Madison, WI 53706
56. G. Logan, Lawrence Livermore National Laboratory, P.O. Box 5511 (L-644) Livermore, CA 94550
57. D. M. Meade, Princeton Plasma Physics Laboratory, P.O. Box 451, Princeton, NJ 08544
58. G. H. Miley, Nuclear Engineering Department, University of Illinois, Urbana, IL 61801
59. D. B. Montgomery, Massachusetts Institute of Technology, Plasma Fusion Center, 167 Albany Street, Cambridge, MA 02139
60. R. R. Parker, Massachusetts Institute of Technology, 170 Albany St., NW 16-288, Cambridge, MA
61. D. E. Post, Princeton Plasma Physics Laboratory, P.O. Box 451, Princeton, NJ 08544
62. P. H. Rebut, JET Joint Undertaking, Abingdon, Oxon, OX14 3EA, England

63. D. Ross, The University of Texas at Austin, Fusion Research Center, Austin, TX 78712
64. P. H. Rutherford, Princeton Plasma Physics Laboratory, P.O. Box 451, Princeton, NJ 08544
65. D. D. Ryutov, Institute of Nuclear Physics, Siberian Branch of the Academy of Sciences of the U.S.S.R., Sovetskaya St. 5, 630090 Novosibirsk, U.S.S.R.
66. W. Sadowski, Office of Fusion Energy, Office of Energy Research, ER-55 Germantown, U.S. Department of Energy, Washington, DC 20545
67. J. A. Schmidt, Princeton Plasma Physics Laboratory, P.O. Box 451, Princeton, NJ 08544
68. W. M. Stacey, Jr., Georgia Institute of Technology, Fusion Research Center, Atlanta, GA 30332
69. R. D. Stambaugh, GA Technologies Inc., P.O. Box 85608, San Diego, CA 92138
70. D. Steiner, Rensselaer Polytechnic Institute, Department of Nuclear Engineering, Troy, NY 12181
71. P. M. Stone, Office of Fusion Energy, Office of Energy Research, ER-55 Germantown, U.S. Department of Energy, Washington, DC 20545
72. V. T. Tolok, Kharkov Physical-Technical Institute, Academical St. 1, 310108 Karkov, U.S.S.R.
73. R. Varma, Physical Research Laboratory, Navrangpura, Ahmedabad, India
74. H. Weitzner, 251 Mercer St., New York University, New York, NY 10012
75. Bibliothek, Max-Planck-Institut fur Plasmaphysik, D-8046 Garching bei Munchen, Federal Republic of Germany
76. Bibliothek, Institut fur Plasmaphysik, KFA, Postfach 1913, D-5170 Julich, Federal Republic of Germany
77. Bibliotheque, Service du Confinement des Plasmas, CEA, B.P. No. 6, 92 Fontenay-aux-Roses (Seine), France
78. Documentation S.I.G.N., Department de la Physique du Plasma et de la Fusion Controlee, Association EURATOM-CEA, Centre d'Etudes Nucleaires, B.P. 85, Centre du Tri, 38041 Grenoble, Cedex, France
79. Library, Centre de Recherches en Physique des Plasmas, 21 Avenue des Bains, 1007 Lausanne, Switzerland
80. Library, Culham Laboratory, UKAEA, Abingdon, Oxfordshire, OX14 3DB, England
81. Library, FOM Instituut voor Plasma-Fysica, Rijnhuizen, Jutphaas, Netherlands
82. Library, Institute of Physics, Academia Sinica, Beijing, Peoples Republic of China
83. Library, Institute for Plasma Physics, Nagoya University, Nagoya 464, Japan

84. Library, International Centre for Theoretical Physics, Trieste, Italy
85. Library, JET Joint Undertaking, Abingdon, Oxfordshire, OX14 3DB, England
86. Library, Laboratorio Gas Ionizzati, Frascati, Italy
87. Plasma Research Laboratory, Australian National Laboratory, P.O. Box 4, Canberra, ACT 2000, Australia
88. Thermonuclear Library, Japan Atomic Energy Research Institute, Tokai, Naka, Ibaraki, Japan
89. Library, Plasma Physics Laboratory, Kyoto University, Gokasho Uji, Kyoto, Japan
90. Office of the Assistant Manager for Energy Research and Development, Department of Energy, Oak Ridge Operations, Oak Ridge, TN 37830
91. F. L. Ribe, College of Engineering, University of Washington, AERL Bldg. FL-10, Seattle, WA 98195
92. J. A. Maniscalo, TRW, 1 Space Park (R1/2128), Redondo Beach, CA 90278
93. D. Overskei, GA Technologies Inc., P.O. Box 85608, San Deigo, CA 92138

94–228. Given distribution as shown in TIC-4500, Magnetic Fusion Energy (Distribution Category UC-20 a,d,f,g: Plasma Systems, Fusion Systems, Experimental Plasma Physics, Theoretical Plasma Physics)